

THESIS FOR THE DEGREE OF LICENTIATE OF ENGINEERING

Surface Charge Dynamics on Polymeric Insulating Materials for High Voltage Applications

Shahid Alam



High Voltage Engineering
Department of Material and Manufacturing Technology

CHALMERS UNIVERSITY OF TECHNOLOGY

Gothenburg, Sweden 2014

Surface Charge Dynamics on Polymeric Insulating Materials for High Voltage Applications

Shahid Alam

© Shahid Alam, 2014.

ISSN 1652-8891

Technical report no. 97/2014

High Voltage Engineering
Department of Material and Manufacturing Technology
Chalmers University of Technology
SE-41296 Gothenburg
Sweden
Telephone + 46 (0)31-772 1000

Chalmers Bibliotek, Reproservice
Gothenburg, Sweden 2014

Surface Charge Dynamics on Polymeric Insulating Materials for High Voltage Applications

Shahid Alam

Department of Material and Manufacturing Technology
Chalmers University of Technology

Abstract

To meet increasing demands in electric energy, it is essential to enhance production of electricity from renewable energy sources (solar, wind and hydro). Such generation sites, however, are usually separated from consumption sites by long distances. An efficient transportation of energy requires implementations of high voltage direct current (HVDC) transmission systems, which operate today at rated voltages up to ± 800 kV. To provide electric insulation for such voltage levels, polymeric insulators are preferable due to a number of advantages over traditionally used ones made of glass or porcelain. The use of polymers, however, leads to surface charging and charge dynamics on insulating elements, which are inherent phenomena in HVDC insulation systems. Thus, knowledge about these processes is essential for proper insulation design, testing and co-ordination. Therefore, the conducted research aimed at providing information about fundamental mechanisms of electric charge transport in HVDC insulation and focused on analyzing roles of gas phase and properties of solid materials on surface charge dynamics.

The study was conducted utilizing flat samples of several types of HTV silicon rubber and cross-linked polyethylene, which are widely used in different HVDC applications. The electrical conductivities and dielectric permittivities of the materials were measured in time and frequency domain, respectively. To study variations of surface charges, the samples were exposed to corona generated in air from nearby sharp electrode that yielded accumulation of electric charges on gas-solid interfaces. Surface potentials induced by the deposited charges were measured at different instants after charging that allowed for obtaining surface potential decay characteristics for the studied materials. The measurements were conducted for both polarities of pre-deposited surface charges at different pressures of ambient air that provided a possibility to control the intensity of neutralization of the deposited surface charges by free counter ions present in air and to evaluate relative contribution of this process to the charge/potential decay. It was found that a reduction of air pressure weakened the intensity of the background ionization in gas and led to diminishing amount of free ions. Under these conditions, the contribution of gas neutralization to the total charge decay was reduced and decay mechanisms were determined solely by the properties of solid materials. Effects imposed by bulk and surface conduction in the solid material on surface charge dynamics were studied by means of experimental measurements and computer simulations. The obtained results allowed for evaluating threshold values of the volume and surface conductivities at which these transport mechanisms become essential. It is demonstrated that bulk conduction becomes dominant mechanism of surface potential decay if volume conductivity of the material is above $\sim 10^{-16}$ S/m. The results of the modeling agree well with the measured characteristics if materials' field-dependent conductivities are taken into account. The performed parametric studies also demonstrate that surface conduction may influence the potential decay if the corresponding conductivity exceeded $\sim 10^{-17}$ S.

Keywords: Surface charging, surface potential, decay rate, ambient pressure, gas neutralization, charge transport, electrical conductivity, HVDC insulation.

Acknowledgments

The project work related to surface charge dynamics on polymeric insulating materials for high voltage applications was carried out at the Division of High Voltage Engineering at Chalmers University of Technology. The author acknowledges the financial support provided by the Swedish R&D program ELEKTRA, project number 36132, jointly financed by ABB and the Swedish Energy Agency, as well as the support provided by Chalmers Area of Advance - Energy.

First and foremost my utmost gratitude goes to my supervisor, Associate Prof. Yuriy Serdyuk for his valuable guidance, discussions, inspiration and most of all for his patience. I will always remember his continuous support during the development of my experimental setup. He had motivated me to do more by bringing new ideas, reading and correcting my manuscripts and finally shaping my report. My thanks also go to my examiner and co-supervisor Prof. Stanislaw Gubanski, Head of Division of High Voltage Engineering, for his valuable advice and support. I am extremely thankful to him for keeping an eye on the progress of the project work and critical comments on the outcomes of the conducted experiments.

I would also like to acknowledge the members of the Reference group (Lars Palmqvist, Birgitta Källstrand, Olof Hjortstam) for providing material samples for conducting experiments related to surface charging and potential decay measurements. Furthermore, I appreciate valuable discussions we had during Reference group meetings, which resulted in new ideas and suggestions for better continuation of the project work.

At last, but not least, I would like to thank my wife, my parents, my family members, my colleagues here in the department and my friends for their invaluable support and inspiration to continue this study abroad.

Shahid Alam
Gothenburg, Sweden
September, 2014

Table of Contents

1. Introduction.....	1
1.1 Background.....	1
1.2 Objectives of the project	1
1.3 Outline of the thesis	1
1.4 List of Publications.....	2
2. Literature review	3
2.1 Charging polymeric surfaces.....	3
2.2 Surface charge/potential decay.....	5
2.2.1 Charge/potential decay mechanisms.....	5
2.2.2 Methods of surface charge measurements	7
2.3 Surface potential decay modeling.....	9
2.4 Mathematical model	10
2.4.1 Potential decay due to intrinsic bulk conduction	10
2.4.2 Decay model incorporating space charge current and surface conduction	11
3. Electrical characterization of studied silicon rubbers	13
3.1 Materials types	13
3.2 Experimental setup for electrical conductivity measurement.....	13
3.2.1 Volume conductivity	14
3.2.2 Surface conductivity	16
3.3 Dielectric response	17
3.3.1 Background of dielectric response and its measurement	17
3.3.2 Dielectric response measurements in frequency domain	17
4. Charging by corona in air and surface potential decay measurements	19
4.1 Experiments	19
4.1.1 Experimental setup	19
4.1.2 Experimental procedure.....	20
4.1.3 Test conditions	21

4.2	Determination of background densities of ions in air at different pressures	22
4.3	Surface charging under different conditions.....	24
4.3.1	Effect of charging voltage magnitude	24
4.3.2	Effect of materials properties	27
4.3.3	Effect of ambient air pressure.....	27
4.4	Surface potential decay	28
4.4.1	Potential decay at different pressures of ambient air	28
4.4.2	Influence of material properties	33
4.5	Evaluation of materials properties from potential decay characteristics.....	35
4.5.1	Field dependent bulk conductivities	36
4.5.2	Trap density distributions	39
5.	Potential decay modeling.....	41
5.1	Physical background and computer implementation	41
5.2	Comparison of the experimental and simulation results.....	42
5.3	Effects of material properties on surface potential decay.....	43
5.3.1	Analysis of effect of bulk conductivity	43
5.3.2	Contribution of surface conduction to potential decay.....	43
5.3.3	Space charge effect	45
6.	Surface charge/potential decay on XLPE	47
6.1	Electrical conductivity and dielectric response of XLPE	47
6.2	Surface potential decay on XLPE at different air pressures	49
6.3	Field dependent bulk conductivity and trap density distribution in XLPE deduced from surface potential decay characteristics.....	52
7.	Conclusions.....	55
8.	Future work.....	57
	REFERENCES	59

1. Introduction

1.1 Background

To meet increasing demands in electric energy, it is essential to enhance production of electricity from renewable energy sources (solar, wind and hydro). Such generation sites, however, are usually separated from consumption sites by long distances. An efficient transportation of energy requires implementations of transmission systems based on high voltage direct current (HVDC), which is the most suitable technology providing low energy losses. The demand of HVDC with a rated voltage above 600kV and UHVDC with a rated voltage higher 800kV has increased during the last decade. To provide electric insulation for such voltage levels, polymeric insulators are preferable due to a number of advantages over traditionally used ones made of glass or porcelain. The use of polymers, however, leads to intensive surface charging and charge dynamics on insulating elements, which are inherent phenomena in HVDC insulation systems. Furthermore, UHVDC power transmission lines may pass through high mountain areas with altitudes up to ~4300 m [1]. Under such conditions, insulation systems operate at reduced air pressure ~600 mmHg. Equally, the increasing penetration of solid insulating polymers in various HVDC applications [2 – 4] demands reconsideration of design principles of the electrical equipment. Thus, operating constraints are getting rigid and, therefore, knowledge about physical processes associated with charge dynamics on polymeric surfaces become essential for proper insulation design, testing and co-ordination.

1.2 Objectives of the project

The work was conducted aiming at increasing understanding of physical processes associated with surface charge accumulation and dynamics on HV polymeric insulating materials. For this, several types of high temperature vulcanized (HTV) silicon rubber and cross-linked polyethylene were considered. Firstly, the experiments related to electrical characterization of the studied materials were conducted using various measuring techniques. Further, surface charging of material samples with different electrical properties and effects of various materials parameters on surface potential distributions were analyzed. Surface potential decay measurements were performed at different pressures of ambient air to study the relative contribution of gas ions neutralization of surface charges to the total charge decay as well as to analyze solely the influence of solid material properties on surface charge dynamics. Finally, surface potential decay characteristics obtained from experimental studies and simulation model were analyzed in order to explore information about the fundamental mechanisms of charge transport.

1.3 Outline of the thesis

Chapter 2 presents a literature survey on surface charging of polymeric insulators through corona discharges in air. Effects of various parameters on surface charging and physical mechanisms responsible for potential decay are elaborated in the light of previously performed experimental and simulation studies. Also, it includes a review of surface potential measuring techniques and

an outline of a mathematical model of potential decay taking into account charge leakage through material bulk and along gas-solid interface.

Chapter 3 presents the experimental setup used for electrical characterization of different types of HTV silicon rubber samples.

Chapter 4 presents the experimental method used for corona charging of flat HTV silicon rubber samples and analyses effects of charging voltage magnitude, polarity, materials properties and ambient gas pressure on resulting surface potential distributions. Potential decay characteristics obtained at different pressures of ambient air are demonstrated and the effects of various parameters are analyzed. Further, decay rates, field dependent bulk conductivity and distribution of trap density deduced from the characteristics for the studied materials are presented and discussed.

Chapter 5 focuses on simulations of surface potential decay accounting for charge leakage through material bulk and along gas-solid interface. A comparison is made between the experimental results and output from the performed simulations. Further, results of a parametric study aiming at identifying the influences of the volume and surface conductivities of the materials as well as the effect of a space charge in the bulk on surface potential decay are examined.

Chapter 6 focuses on an analysis of physical mechanisms responsible for potential decay on cross-linked polyethylene (XLPE) material sample which represents a material with extremely high intrinsic resistivity. The influence of different parameters like air pressure, material properties and polarity of surface potential on the charge decay is analyzed. Further, field dependent bulk conductivity and distribution of trap density extracted from the potential decay rates are presented and discussed.

Chapter 7 presents conclusions drawn from the experimental and simulation results.

Chapter 8 includes suggestions to continuation of the work.

1.4 List of Publications

The performed studies are summarized in the following scientific publications.

- ❖ S. Alam, Y. Serdyuk and S. M. Gubanski, “Surface potential decay on silicon rubber samples at reduced gas pressure”, Proceedings of 23rd Nordic Insulation Symposium, Trondheim, Norway, pp. 19-22, 2013.
- ❖ S. Alam, Y. Serdyuk and S. M. Gubanski, “Potential Decay on Silicone Rubber Affected by Bulk and Surface Conductivities”, IEEE Transaction on Dielectrics and Electrical Insulation, 2014, under reviewing.
- ❖ S. Alam, Y. Serdyuk and S. M. Gubanski, “Contribution of Gas Neutralization to the Potential Decay on Silicon Rubber Surfaces at different Ambient Pressures”, International Conference on High Voltage Engineering and Applications (ICHVE 2014), September 8-11, 2014, Poznan, Poland, accepted.

2. Literature review

This chapter presents a literature review on surface charging of polymeric insulators through corona discharges in air. Physical mechanisms responsible for charge/potential decay on pre-charged insulating materials are highlighted based on previously performed experimental and simulation studies. Further, a mathematical model of potential decay taking into account charge leakage through material bulk and along gas-solid interface is discussed.

2.1 Charging polymeric surfaces

High voltage polymeric insulators (line- and post-insulators, bushings, cable terminations etc.) operating under dc high voltages are normally exposed to electric stresses which provide conditions for deposition and accumulation of charged species (ions) on gas-solid interfaces. The accumulated surface charges may become strong enough to alter field distribution around an insulator, which in turn may affect its performance [5 - 8]. For a proper design of insulation, it is therefore important to understand processes associated with charge dynamics on polymeric surfaces.

Surface charging of polymeric materials have been studied extensively especially during last couple of decades due to development of new HVDC systems for ultra-high voltage levels. Effects of various parameters like voltage amplitude, polarity, time duration, geometry of an insulating system as well as environmental factors on surface charge accumulation and its distribution along the surface have been elucidated [3, 7, 9]. It has been shown that deposition and relaxation of surface charges are affected by properties of both phases, i.e., solid material (such as transverse (surface) and longitudinal (bulk) electrical conductivities, permittivities) and parameters related to surrounding gas medium (e.g., conduction due to free ions, rate of ion pair generation by natural radiation and electric field distribution within the gas phase) [8, 10, 11]. Further, it was demonstrated that in most of practical cases surface charging cannot be explained by considering only one mechanism and it is a result of competitive action of several processes activated during high voltage application [7].

Despite of the core information on surface charge accumulation and relaxation in HV systems obtained in previous studies, newly emerging applications require more detailed knowledge and more complete understanding of associated physical processes. A number of unclear questions arising from practical use of polymeric insulators related to the surface charge deposition, charge behavior with respect to time, dynamics changes of electric field due to charge deposition on various HVDC equipment [12], different factors influencing surface charge accumulation etc. are still required to be properly addressed. From the documented literature, it is commonly accepted that phenomena associated with surface charge accumulation involve several physical mechanisms (polarization and conduction, external discharges, etc.) and each of them may become dominant under certain conditions [9, 13, 14].

Corona charging

Surface charging of insulation materials may be achieved by different techniques such as corona charging, contact charging, use of an electron beam, polarization, exposing an insulator to high voltages providing conditions for accumulation of free ions present in air, partial discharges in the surrounding gases due to strong electric fields etc. [9, 15, 16]. Among these techniques, corona charging has appeared to be most popular due to its simplicity and high repeatability of results. It is also utilized in the present study.

Corona is a self-sustainable, non-disruptive localized electrical discharge in gas that can be achieved by connecting electrodes with small surface curvature (e.g. sharp edges) to a high voltage source. Needle-plane or wire-plane are typical examples of such electrodes configurations providing highly non-uniform electric field distributions and, thus, giving rise to localized electrical discharges [9]. If material samples are placed in the vicinity of such electrode system, deposition of generated charged species may take place on its surface. One should note that using simple point (needle) - plane electrode arrangements as a way of charging solid material surfaces provides uneven distribution of charges on gas-solid interfaces that is typical for practical cases. If a uniform surface charging is required, a more advanced approach based on the use of a corona triode (where a metallic grid is inserted in the gap between the corona electrode tip and the material surface) is usually utilized [9].

The localized discharges in the vicinity of sharp points in air appear due to high electric field stresses stimulating electron impact ionization of molecules of surrounding gas and, as a result, leading to an increased amount of charged species (ions) of both the polarities. The threshold for the corona discharge depends on the availability of free electrons, produced due to background gas ionization, which can trigger an electron avalanche. The ionic species generated in the ionization zone move towards counter electrodes in the applied electric field provided by the electrodes and eventually enter into a low field region (so-called drift region), where further ionization is suppressed. Under certain conditions, e.g. at voltages of sufficiently high amplitudes, electron avalanches in the ionization volume may surpasses a critical length X_c and produce space charge strong enough for development of a plasma channel (streamer), which can extend in both directions (towards anode and cathode). From measurements [17], it has been found that such transformation occurs when the number of charge carriers within the electron avalanche head reaches a critical value $n = \exp(\alpha X_c) = 10^8$, here α is the ionization coefficient. Under such conditions a complete breakdown usually occurs. For the purposes of solid material surface charging, such situation must be avoided.

The type of ions generated in positive and negative coronas in gas depends on its nature [9]. To identify their types in air, spectrometric studies for both positive and negative coronas have been performed [18, 19]. It has been found that chemical composition of produced charges is quite complex and strongly depends on the amount of moisture (H_2O molecules) in gas. Thus, dominant species produced in positive corona in air are clusters of type $(H_2O)_n H^+$, where the integer n increases with relative humidity. At low humidity, other species such as $(H_2O)_n NO^+$ and $(H_2O)_n (NO_2)^+$ are found to be dominant. In case of negative corona in air, the dominating species are CO_3^- ions, although other ionic species such as O^- , O_3^- and NO_2^- are also found and their relative fractions are highly dependent on air pressure. Moreover, at atmospheric pressure and 50% of relative humidity, about 10% of the ions are in the hydrated form $(H_2O)_n CO_3^-$. Thus, effects of the environmental factors such as humidity, temperature and pressure on the nature of

generated ions in the vicinity of the corona treated materials are important to investigate, so that to find the correct ion species deposited on polymeric surfaces.

If polymeric material is placed in the vicinity of a corona source, ionic species and free charge carriers present in the atmosphere may experience forces driving them towards solid surfaces where they may be partially trapped and/or injected into the bulk, thus charging the material surface. From the previous works of several authors [20, 21] related to charge trapping, it has been made possible to show that polymeric surface contains both deep and shallow surface traps (note that the depth characterizes energy level). The authors proposed that the ions generated e.g. in a corona discharge, once come to the surface of polymeric materials, can either stay as stable entities on the surface or can be distributed according to the energy states of the ions and surface thus forming surface charge layers. It is claimed also that transfer of electrons might occur to neutralize the ions, thus charging the surface state of the polymer to the same charge as the incident ions.

2.2 Surface charge/potential decay

Measurements of surface potential decay on corona charged polymeric materials is a powerful tool to electrically characterize highly resistive (insulating) materials and can be used e.g. as a complementary method to traditional techniques. It also allows to evaluate materials charging methods and various electrical processes associated with charge/potential decay such as charge transport, trapping/detrapping, neutralization and recombination.

Surface potential decay on insulating materials due to relaxation of pre-deposited surface charges has been studied extensively in relation to GIS equipment. During last couple of decades, the interest to this subject has raised significantly due to development of components for HVDC power transmissions. The conducted research focused at evaluations of effects of material properties, geometrical arrangements, surrounding gasses and environmental factors, such as humidity and temperature [2, 16, 22, 23]. Based on results of the performed studies, different mechanisms and theories have been proposed to describe surface charge decay, e.g. in terms of charge transport within the material, charge spreading over its surface, etc. [24 - 27]. The potential decay characteristics have been treated in different formats, e.g. utilizing so-called “V vs. time” and “log(V) vs. log(time)” dependencies in order to elucidate quantitative interpretation of the initial stages of the decay as well as to discuss cross-over phenomenon in surface potential decay curves [15, 28]. In addition, different hypothesis and various models have been suggested to describe surface charge dynamics [6, 15, 25, 28]. Despite of all the efforts made, there is still a lack of knowledge in the subject due to continuous development of hybrid gas-solid insulation systems for various HVDC applications and extensive use of new materials [2 - 4]. Therefore, further investigations are required to dig the research area and to contribute to the available knowledge.

2.2.1 Charge/potential decay mechanisms

Electric charges deposited on surfaces of insulating materials, e.g. by utilizing corona charging techniques, induce a potential on the surface that changes with respect to time. The charge can either flow out in the longitudinal or transverse directions to the surface or it can be compensated by the appearance of charges of opposite polarity (bonded or free) at gas-solid interface due to the electric field setup by the surface potential. From the documented literature on the charge decay, it is commonly accepted that the amount of charges on a polymeric surface under normal

conditions can diminish due to several processes, namely, bulk [3, 24, 26] and surface [29, 30] conduction in the solid material and due to arrival of free counter ions present in the gas phase [6, 31 - 33]. The latter mechanism is usually referred to as a gas neutralization in the literature. It is dependent on many factors like the amount of free ions in the gas, conditions of their drift and diffusion, extension of the so-called capturing volume, etc. [31]. It has been shown [6] that contribution of gas neutralization to charge decay may become significant (and even deterministic) especially for highly resistive materials at high magnitudes of the potentials induced by deposited surface charges. Similarly, the role of surface conduction in the potential decay can be enhanced due to material aging [34] and high humidity [30, 23, 35]. Under normal conditions, all three decay mechanisms act simultaneously and it is hard to distinguish between their relative contributions to the total effect that is highly desirable for understanding of the phenomenon. Though it is not clear which mechanism is more dominant, it is a point of worth to explore the relative importance of each mechanism.

Bulk neutralization

Bulk neutralization of surface charges may appear due to the intrinsic conduction, polarization processes, charge injection and trapping/detrapping in the bulk of the solid material [15]. Most of recent theories of surface charge decay assume that during and immediately after surface charge deposition it is injected into the material and transported through its bulk that is accompanied by slower processes of volume polarization [24]. From another side, intrinsic conduction may also play significant role because it depends on the amount of transported charges defined by the rate of charge carriers generation, intensities of charge trapping, de-trapping, recombination as well as mobility of carriers within the material bulk [21, 36]. In this context, it is worth noting that intrinsic conduction is in general field dependent and is often considered as negligible under low fields and moderate temperatures [25].

The relative contribution of the physical processes inside the material bulk to the total charge decay has been evaluated with the help of various mathematical representations. Thus, it has been shown in [16, 28] that exponential decay characteristics are typically associated with intrinsic conduction process while other mechanisms (charge injection, slow polarization, etc.) result in power law type dependences.

Surface conduction

Surface conduction refers to the charge leakage along the insulator surface. It is highly field dependent (surface current is usually zero at low fields) [25]. The leakage current take place due to a tangential component of the electric field activated due to a potential gradient along the material surface, and is quantified by surface conductivity [30]. This mechanism dominates mostly under initial stage of surface charge decay [25]. The surface leakage strongly depends on the material ageing and air humidity. This process may only cause in a lateral spread of the charge causing a more uniform potential distribution, however, the total charge on the surface may remain the same [31].

Gas neutralization

The term “gas neutralization” refers to the compensation or neutralization of surface charges due to arrival of free counter ions present in gaseous medium [31, 37]. Free ions of both polarities exist in the air due to various background ionization processes. Electric field setup by the surface

charges within the surrounding gas volume can lead to electrostatic forces attracting the ions to the surface. The arrival and accumulation of free ions results in a reduction of a surface potential. Concentration of free ions and strength of electric field in the vicinity of a charged sample are critical factors which determine the efficiency of surface charge decay due to gas neutralization [6, 31].

2.2.2 Methods of surface charge measurements

Presence of electrostatic charges on surfaces of polymeric materials can be detected using different techniques which can be split on qualitative and quantitative methods. Thus qualitatively, the polarity and relative magnitude of surface charges can be detected by using an electrostatic powder which is typically a mixture of two different types of particles e.g. talc and jewelers' rough. The powder, when put on a surface that is charged positively, attracts talc particles while rough particles are attracted to surfaces with opposite polarity. An increased amount of the attracted particles indicate locations on the surface with enhanced surface charging. Due to its nature, this method may provide qualitative information on charge polarity and surface charge distribution but other parameters, e.g. on decay of surface charges can't be obtained [38]. Quantitative evaluations can be based on measurements of induced electric fields or electrostatic potentials and there is a variety of instruments utilizing contact or contactless methods. The latter is the most attractive for research purposes and are implemented in potential probes and electrostatic fieldmeters [39] allowing for conducting measurements of static and dynamic quantities.

Most of the potential probes are of capacitive type. Their working principle is to detect charge quantity electrostatically induced on the detecting electrode of the probe. When brought closer to surface under test as show in Figure 2.1, the charged sample induces a floating potential on the plate depending on the capacitive coupling between surface and the probe. Thus, the potential on the probe is a ratio of induced charges to the capacitance between the probe and surface. Therefore, any changes in the distance may cause a flow of current in either direction in order to adjust the voltage on the probe. By measuring the current I and distance d , the actual charge density on the analyzed surface can be determined [40]. Sensitivity of such devices should be

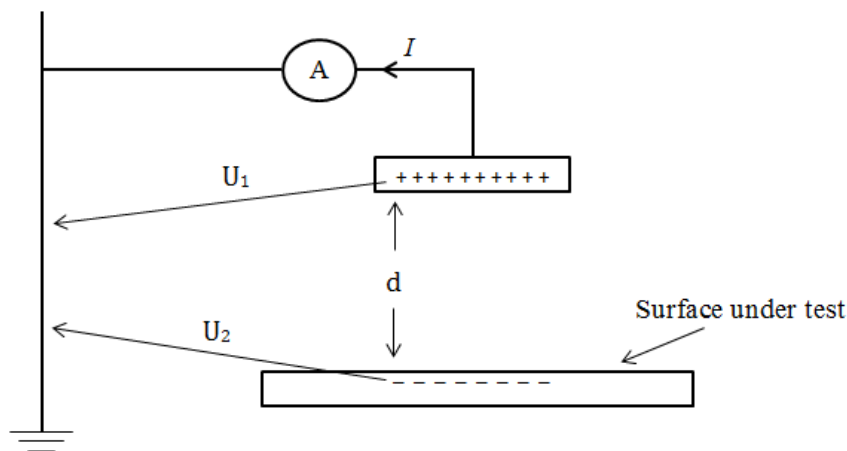


Figure 2.1. Schematic view of a capacitive probe.

high enough to detect small changes in the current amplitudes due to its strong dependence on the probe to surface distance. A schematic diagram of a capacitive probe is shown in Figure 2.1.

Another method called “field-nullifying technique” has been developed, which is mostly used for flat charged samples. Kelvin’s type electrostatic probes are based on such techniques. In this method, a variable voltage source is connected to a vibrating sensor through a feedback loop. Vibrations of the sensor result in a certain current that can flow in or out from the probe. When the probe approaches the analyzed surface, voltage on the sensor through the feedback loop is adjusted in such a way that current approaches zero. Zero current detection means that the probe voltage is the same as the charged sample voltage. Since the gradient of the potential defines electric field, zero potential difference between the probe body and the charged surface means no electric field between them. Therefore, this method is called “field nullifying technique”. Major advantages of using Kelvin’s probe are: (1) physical state of the object under test does not change and also modification of charges on the surface is minimized due to its non-contact nature, (2) unlike the capacitive probe, surface to probe distances, if changed within a few mm, don’t have a significant effect on the measurements of actual surface potential and a good resolution can be maintained. A schematic diagram of the probe utilizing field-nulling technique and its equivalent capacitances are shown in Figure 2.2.

Although surface potential measurements are easy and fast to perform using electrostatic voltmeters, the quantification of the measured results is not always simple. In order to extract surface charge densities from measured potential magnitudes, analytical and numerical relations should be sometimes carefully considered in order to obtain meaningful values [39]. Thus for flat material samples, as shown in Figure 2.2, the situation during the potential measurement corresponds to open circuit configuration, where the electric field between the probe and the surface is zero. Therefore, surface charges can be coupled only to the grounded electrode [28, 41]. Assuming steady state conditions when initial polarization is stabilized (thus a material can

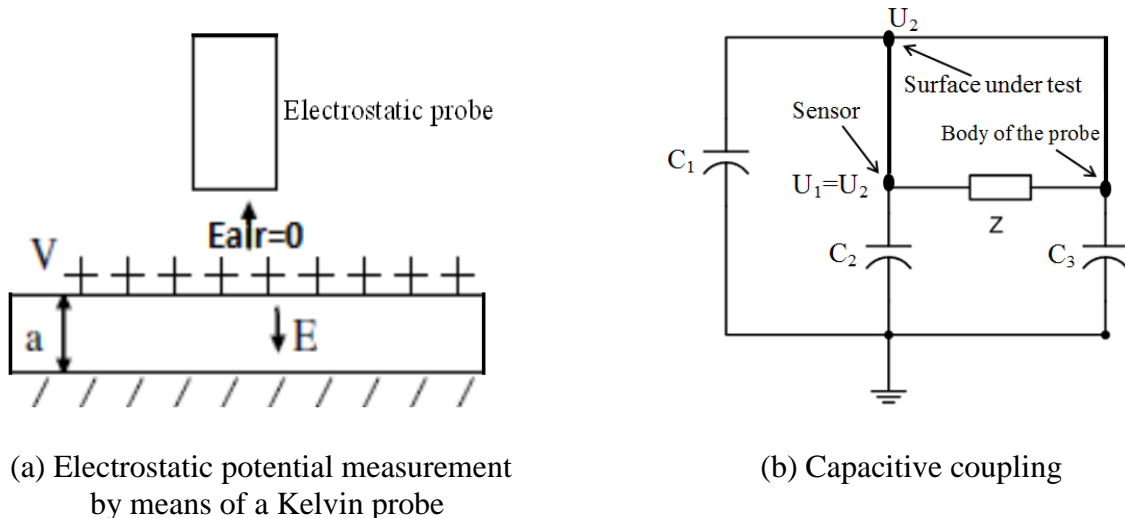


Figure 2.2. Kelvin probe placed above a charged surface. Capacitances C_1 , C_2 and C_3 represent the surface to ground, sensor to ground and body of the probe to ground respectively.

be modelled by a constant permittivity) and neglecting space charge effect, a surface potential V_s due to uniform surface charge density σ_s can be presented as

$$V_s = \frac{L}{\epsilon} \sigma_s \quad (2.1)$$

Here, L is the thickness and ϵ is the permittivity of the material sample. Potential to charge conversion for cylindrical and other geometries involve complex numerical calculations for determining probe response functions.

2.3 Surface potential decay modeling

Potential decay mechanisms, described in section 2.2.1, are not the only physical processes inside the material bulk and on the gas insulated interface that cause decay of charges deposited on surfaces of insulating materials. Other possible sources that can contribute to the potential decay are di-electric relaxation of insulating materials and space charge accumulation in the material bulk. Taking into account all the possible decay mechanisms, the general equation can be derived as

General potential decay equation

Consider a plane insulator of thickness L placed on a grounded electrode on one side, the other surface is free and is large enough as compared to the thickness so that the side effects can be neglected. Under such conditions, surface charge densities, field and potential are functions of the distance to ground only [28]. Assuming that the surface is charged instantly at time $t = 0$ (by e.g. corona) to an initial voltage V_s and afterwards is kept in open circuit configuration ($E=0$ outside the sample that is satisfied during measurements using Kelvin probe). For this situation, a continuity equation for a current density can be written for any point of the insulation [15]

$$\frac{\partial D}{\partial t} + K_v E + \sum_i \mu_i \rho_i E = 0 \quad (2.2)$$

Here, the first term is the time derivative of the electric displacement $D = \epsilon_0 E + P$ defining the displacement current density (ϵ_0 is the permittivity of vacuum, E is the electric field and P is the polarization vector). The second term represents the current density due to intrinsic conductivity K_v of the dielectric material. The third term describes the current density due to additionally injected charge carriers into the material bulk, μ_i and ρ_i being the mobility and charge density of the particular injected charge carrier respectively. It can be noticed that equation (2.2) is valid only in case of zero gas neutralization. Further, contribution from the surface conduction should be taken into account in order to get a more insight into equation (2.2).

In the present study, a mathematical model of potential decay neglecting gas naturalization and taking into account the charge leakage through material bulk and along gas-solid interface is adopted as discussed in the following sections.

2.4 Mathematical model

A relationship between the rates of variations of surface charge density $\sigma_s(\text{C/m}^2)$ and induced surface potential V_s (V) for flat material samples and zero field induced in air (provided by the measuring probe) can be derived from Gauss law and can be written as [42]

$$\frac{d\sigma_s(t)}{dt} = \frac{\varepsilon_r \varepsilon_0}{L} \frac{dV_s}{dt} \quad (2.3)$$

Here, t stands for time, ε_0 is permittivity of vacuum, ε_r is the relative permittivity of the material. At the same time, the rate of change of the surface charge density can be linked to charge sources and sinks by utilizing current conservation conditions. Thus assuming leakage of deposited charges along gas-solid interface and through the solid material bulk as well as their neutralization by gas ions, one may write

$$\frac{d\sigma_s(t)}{dt} = -j_s(t) - j_b(t) - j_g(t) \quad (2.4)$$

Here, j_s is the current density due to surface conduction, j_b is the current density due to bulk conduction and j_g is the current density caused by gas ions arriving to gas-solid interface and neutralizing surface charges. The latter term can be ignored in the present study due to the especially designed experimental setup, where the involvement of the gas phase is minimized by reducing air pressure (see sections 4.2 below). The reduced ambient pressure inside the test vessel causes weaker background ionization, which yields lower amount of free ions in air making gas neutralization negligible.

2.4.1 Potential decay due to intrinsic bulk conduction

In case of negligible surface conduction and space charge accumulation in the solid, inserting (2.4) into (2.3) allows for considering only intrinsic conduction within the material bulk and transforms the potential decay equation (2.2) into a very simple form that is given as

$$\frac{\partial V_s}{V_s \partial t} = - \frac{K_v}{\varepsilon_0 \varepsilon_r} \quad (2.5)$$

Solution of equation (2.5) with a constant intrinsic conductivity yields an exponential shape of the potential decay with a time constant equal to the ratio between the intrinsic conductivity and permittivity (K_v/ε). The conductivity $K_v = \sum q\mu n$ is proportional to the product of the charge carrier density n and their mobility μ . The latter quantities may change depending upon the internal field strength in the material that makes it necessary to consider some hypotheses on the processes leading to such variations in order to rely on the solution of equation (2.5) [28].

As shown in previous works [40, 43], surface potential decay on highly resistive materials can be associated with bulk conduction. In these studies, the intrinsic conductivity of the materials is assumed to be field-dependent and is represented utilizing Poole-Frenkel model. According to this approach, charges being deposited on material surface stimulate an electric field and thus a

current inside the material bulk that increases exponentially with the square root of surface potential for high electric fields [44]. This kind of behavior can be described mathematically as

$$K_v(V_S) = K_{v0} e^{\beta\sqrt{V_S}} \quad (2.6)$$

Here, $K_v(V_S)$ is the field (or potential) dependent bulk conductivity, K_{v0} is a zero-field limit value, and β is the Poole-Frenkel factor. The parameters in equation (2.6) can be calculated by plotting $K_v(V_S)$ as a function of square root of surface potential and by fitting the variations of the field dependent bulk conductivity with exponential function. A theoretical value of β can be estimated from equation (2.7) which is given as

$$\beta = \frac{q}{kT} \sqrt{\frac{q}{\pi\epsilon L}} \quad (2.7)$$

Here, q is the elementary charge; k is Boltzmann's constant, and T stands for temperature. As seen, the theoretical value of β is dependent on the material thickness and permittivity. In [40], a fairly good agreement was found between the theoretical and experimental values of β except for material samples with high percentage of additional fillers. Concerning the quantitative contribution of bulk conduction, it has been shown in the previous studies that intrinsic conductivity of the insulating material, naturally enhanced at higher magnitudes of surface potential, can fully describe the charge decay and surface potential kinetics observed experimentally [43].

2.4.2 Decay model incorporating space charge current and surface conduction

Injection of charges, deposited on the gas solid interfaces of dielectrics, into the material bulk is considered as a strong argument to explain the cross-over phenomena [15]. Many surface potential decay models are based on the charge injection hypothesis [24, 28]. According to [42, 45, 46], the steady state bulk current density can be divided into two regimes that are given as

$$j_{Bulk}(V_S) = \begin{cases} j_{ohmic}, & V_S < V_{ST} \\ j_{SCLC}, & V_S > V_{ST} \end{cases} \quad (2.8)$$

Here, j_{ohmic} and j_{sclc} are the ohmic and space charge limited current (SCLC) densities, respectively, and V_{ST} is the transition voltage. The SCLC is due to the charge injection through the gas-solid interface and its transport thorough the material bulk, which was found to be more efficient at high fields and fine thickness of the material samples [45, 47]. In [45], the two current regimes are reported to be separated at around -950V and material thickness of 27 μm . In [47, 48], it has been shown that the two current densities inside the material can be approximated as

$$J_b = \frac{K_v V_S}{L} + \frac{9}{8} \epsilon_0 \epsilon_r \mu \frac{V_S^2}{L^3} \quad (2.9)$$

The first term on the right hand side of (2.9) describes ohmic conduction while the second term represents the SCLC (μ stands for the mobility of charge carriers).

For non-uniform potential distributions, a potential gradient exist along the surface that stimulates lateral spread of the charges. Mathematically, the surface current density can be represented as [30, 42]

$$J_s = -K_s \frac{d^2 V_s}{ds^2} \quad (2.10)$$

Here, K_s is the surface conductivity. In (2.10), the derivative along the gas-solid interface (s) is to be considered.

Inserting (2.9) and (2.10) into (2.4) and accounting for (2.3) yields the equation for the potential decay

$$\frac{\partial V_s(t)}{\partial t} = \frac{L \cdot K_s \cdot d^2 V_s(t) / ds^2}{\epsilon_0 \epsilon_r} - \frac{K_v V_s(t)}{\epsilon_0 \epsilon_r} - \frac{9}{8} \cdot \mu \cdot \frac{V_s(t)^2}{L^2} \quad (2.11)$$

Equation (2.11) is one of the possible representations of potential decay mechanisms that accounts for charge leakage through material bulk and along gas-solid interface.

Providing a strong physical background for equation (2.11), its implementation and output from the simulation are discussed in chapter 5.

3. Electrical characterization of studied silicon rubbers

This chapter focuses on electrical characterization of different types of HTV silicon rubber samples utilizing various measuring and diagnostic instruments. Material types and their properties as well as experimental setup used for measurement of surface and bulk conductivities are described. Further, measurements of dielectric response and dielectric loss factor for studied materials are presented and discussed.

3.1 Materials types

The measurements were performed on flat samples $100 \times 100 \times L$ mm³ (L stands for the thickness) of different types of high temperature vulcanized silicon rubber (HTV-SR) with additives and fillers that are usually present in the material to meet requirements in diverse high-voltage applications. Thus, these are as follows: two materials cured with peroxide and reinforced with silica filler (A and B) commercially known as Elastosil R401/50 and Elastosil R401/60, two materials peroxide cured filled with 50% and 58% of aluminumtrihydrate (C and D), respectively known as Elastosil R401/50 with ATH and Elastosil R401/40 with ATH and one material cured with platinum catalyst (E) known as Elastosil R4001/50. One type of ATH (50%) used is OL-104 ZO. It is a vinyl-silane treated, finely precipitated aluminium hydroxide. Second type of ATH (58%) is DCLBP (di (2, 4-dichlorobenzoyl) peroxide). Cured material samples had good transparency with shore hardness of 50. Specifications of all the material samples are given in Table 3.1. Note that further below the materials will be mentioned in the text and in the figures as assigned in the table.

3.2 Experimental setup for electrical conductivity measurement

Bulk and surface conductivities of material samples were measured at ambient conditions according to ASTM standard D 257 using Keithley 6517A electrometer equipped with a test

Table 3.1. Specification of the material samples used within the performed study.

Material	Commercial name	Curing agent	Additional filler
A	Elastosil R401/50	peroxide	-
B	Elastosil R401/60	peroxide	-
C	Elastosil R401/50	peroxide	50% ATH
D	Elastosil R401/40	peroxide	58% ATH
E	Elastosil R4001/50	Pt catalyst	-

fixture Keithley 8009. The test fixture has a concentric ring electrode that is configured differently with the help of an integrated toggle switch to measure surface and volume currents. The applied test voltage was 1 kV. The different configurations of the test fixture used during surface and volume current measurements are shown in Figure 3.1.

3.2.1 Volume conductivity

Volume currents for HTV silicon rubbers A, C and E, obtained using electrodes configuration shown in Figure 3.1a are shown in Figure 3.2. As can be seen, time variations of the currents for different materials are dependent on materials compositions. Maximum variations are obtained for material C while minimum ones can be observed for material A. Since material C is heavily doped with ATH, volume polarization may be much higher, therefore, a much higher initial capacitive current is observed. This is further confirmed by permittivity measurements shown in Figure 3.5a. The relaxation of such processes is a time consuming phenomenon, that's why, volume current takes longer time to reach a fairly constant value. In order to mitigate polarization current, the experiments should be conducted for a significantly long time and in the present case even after a time period of 10^5 sec (~ 28 h) the measured current is not purely conductive. One may see that that for material A, which doesn't contain additional filler, the time span is

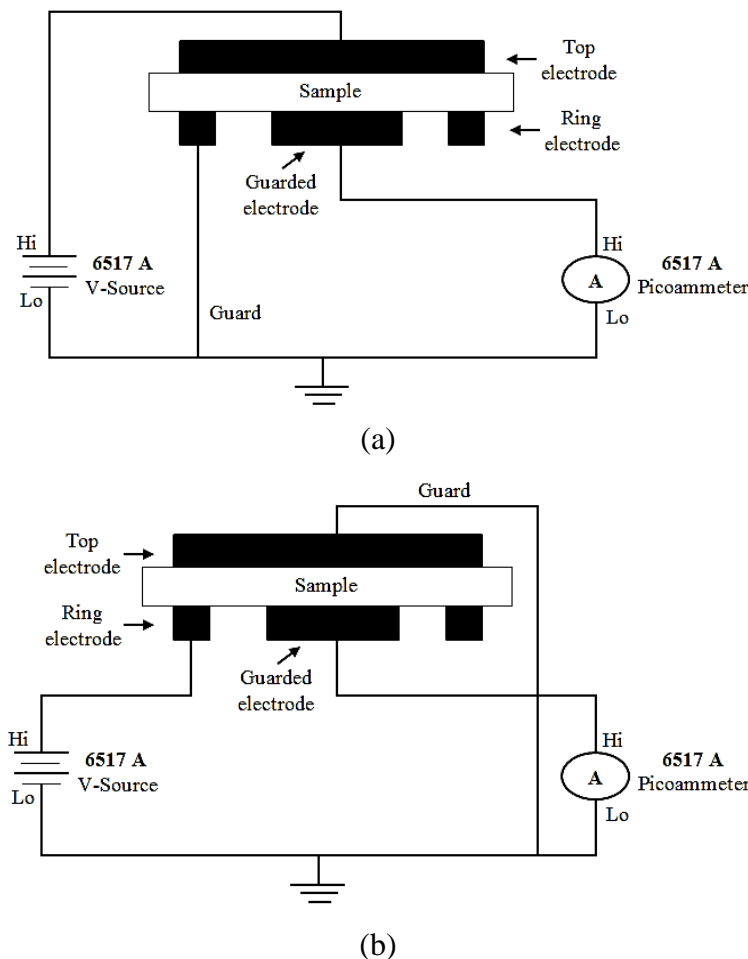


Figure 3.1. Different configurations of the electrodes during bulk conductivity (a) and surface conductivity (b) measurements.

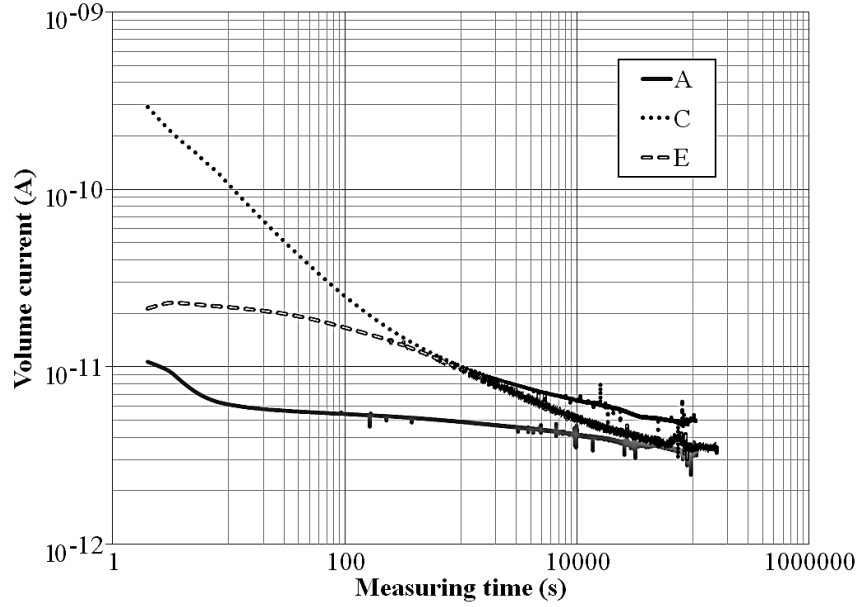


Figure 3.2. Volume currents measured for silicon rubbers A, C and E.

relatively shorter. For silicon rubber E, similar behavior as that of material C is observed, however, the initial magnitude and slope of current time variations are much lower. In all cases, the measurements were stopped after 28 h time period due to practical reasons and the corresponding current magnitudes (which are close to steady-state values) for all the three materials are used to obtain bulk conductivities.

$$K_v = \frac{L}{A} * \frac{I}{V} \quad (3.1)$$

Here L is the thickness of the material sample, A is the area of the electrode configuration, I is the steady state value of the bulk current and V is the applied test voltage. Volume conductivities for

Table 3.2. Volume (K_v) and surface (K_s) conductivities, dielectric constants ϵ_r (at 50Hz) and thickness of samples of the studied materials arranged according to increasing bulk conductivity level.

Material	K_v , S/m	K_s , S	ϵ_r	L, mm
B	1×10^{-15}	5×10^{-19}	2.7	2.0
E	3.5×10^{-15}	6.6×10^{-18}	3.0	2.25
A	3.7×10^{-15}	1.1×10^{-17}	2.4	2.28
C	5.4×10^{-15}	9.5×10^{-18}	3.5	2.29
D	8.5×10^{-14}	3.2×10^{-17}	3.3	2.1

different materials obtained using equation (3.1) are given in Table 3.2. As can be seen, for materials A and E, the apparent steady state currents are almost overlapping, therefore, a corresponding effect can be observed in their respective bulk conductivities.

3.2.2 Surface conductivity

An example of measured surface currents obtained using electrode configuration in Figure 3.1b is shown in Figure 3.3. As can be seen, variations of the currents with respect to time are different for different materials depending on the curing agent and additional fillers. For material A, the current is almost constant while for material C it starts at much higher magnitude that decreases over a certain range of time until it reaches a steady state. The reason could be due to the fact that the additional filler contents of material C causes an increase in the strength of both surface and volume polarization processes. Therefore, immediately after applying test voltage, a capacitive current of approximately one order of magnitude higher compared to other two materials is observed. After the initial spike, polarization processes relaxes with time and finally the current drops to a fairly constant value. For silicon rubber E, similar behavior is noticed, however, the rate of the decrease of the surface current is much lower as compared to that for material C. As seen, the steady state is reached at different times for different material samples. Therefore, diverse instants are selected for various materials to obtain the steady current magnitudes, which are used to obtain the surface conductivity as

$$K_s = \frac{I}{V * 53.4} \quad (3.2)$$

Here I is the steady state value of the surface current and V is the applied test voltage. The constant number “53.4” is the ratio of the effective dimensions of the electrode system. Surface conductivities for different materials obtained using equation 3.2 are given in Table 3.2.

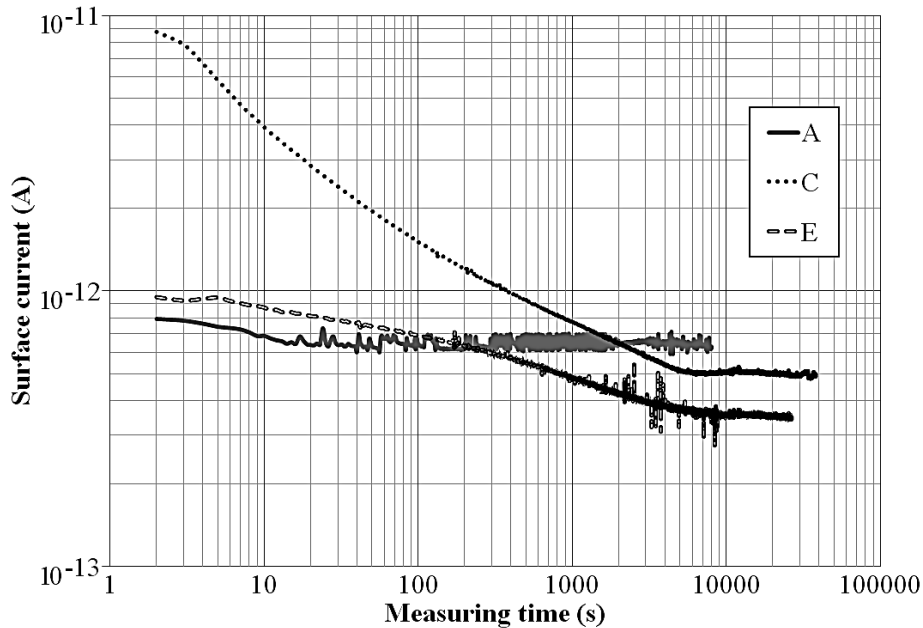


Figure 3.3. Surface currents for materials A, C and E.

3.3 Dielectric response

3.3.1 Background of dielectric response and its measurement

In general, every dielectric material on both the microscopic and macroscopic level consists of balanced amounts of positive and negative charges. When the material is exposed to an external electric field, different mechanisms start to align the bonded charges along the direction of the field, resulting in the polarization of the material. Different polarization mechanisms (electronic, ionic, dipole, interfacial) can contribute at the macroscopic level and each of them may become active in different frequency range or at different time spans. To understand the polarization processes and to be able to interpret results of diagnostic measurements, various models of insulation have been proposed by different authors [49, 50]. An example shown in Figure 3.4 demonstrates the equivalent circuit approach within which a material is represented by a combination of capacitive and resistive elements connected to a high frequency capacitance C_∞ and an insulation resistance R_0 . The different mechanisms of polarization are represented by the series combination of $R_i C_i$ elements with corresponding characteristic time constants [49].

Dielectric response in the time domain can be represented by relaxation (absorption/desorption, charging/discharging, polarization/depolarization) currents, return voltage, discharge voltage and isothermal relaxation current. In frequency domain, it appears as complex capacitance or complex permittivity and dielectric loss factor ($\tan\delta$). As long as the insulation material behaves linearly, there exist algorithms that can be used to convert measurements between time domain and frequency domain [49 - 51].

3.3.2 Dielectric response measurements in frequency domain

The dielectric response measurements were carried out in the frequency range from 0.1 mHz to 1 kHz by means of an Insulation Diagnostic System IDAX 300. The system is equipped with an internal sinusoidal voltage source that can provide voltages up to $200 V_{peak}$ ($140 V_{rms}$). The response current, as a result of the voltage applied to the test object, is measured and used for the calculation of the complex permittivity.

Real and imaginary parts of the complex permittivity measured at different frequencies for HTV silicon rubber samples are shown in Figure 3.5. As can be seen for materials A and E, the real part is nearly constant in the studied frequency window, although absolute values are different for the materials. This indicates that polarization intensity doesn't change in the selected frequency range. On the other hand, for material C, a difference can be observed at low and high frequencies. Such differences can be attributed to the significant content of ATH filler in the material which may activate interfacial polarization at lower frequencies.

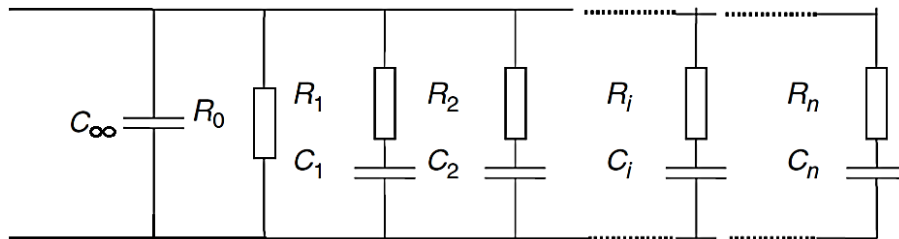
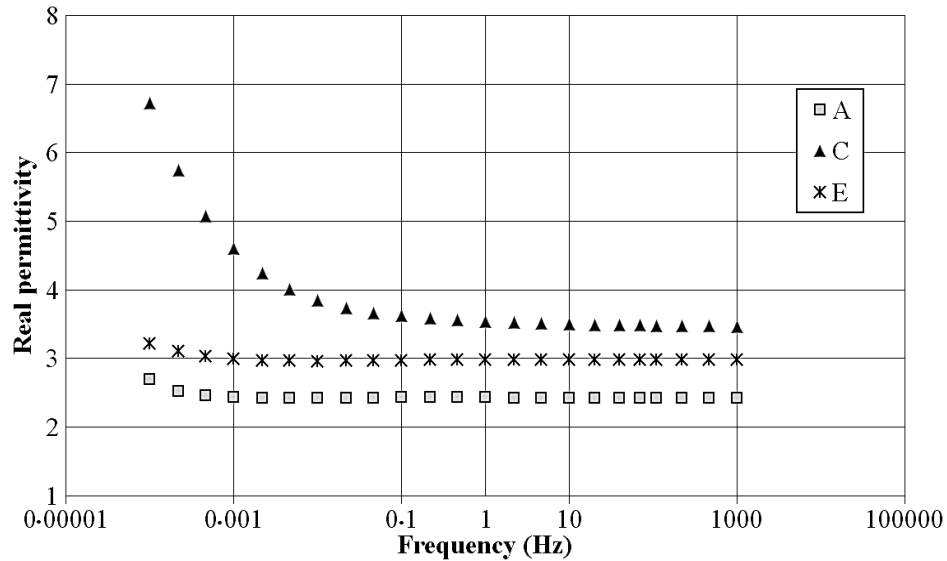
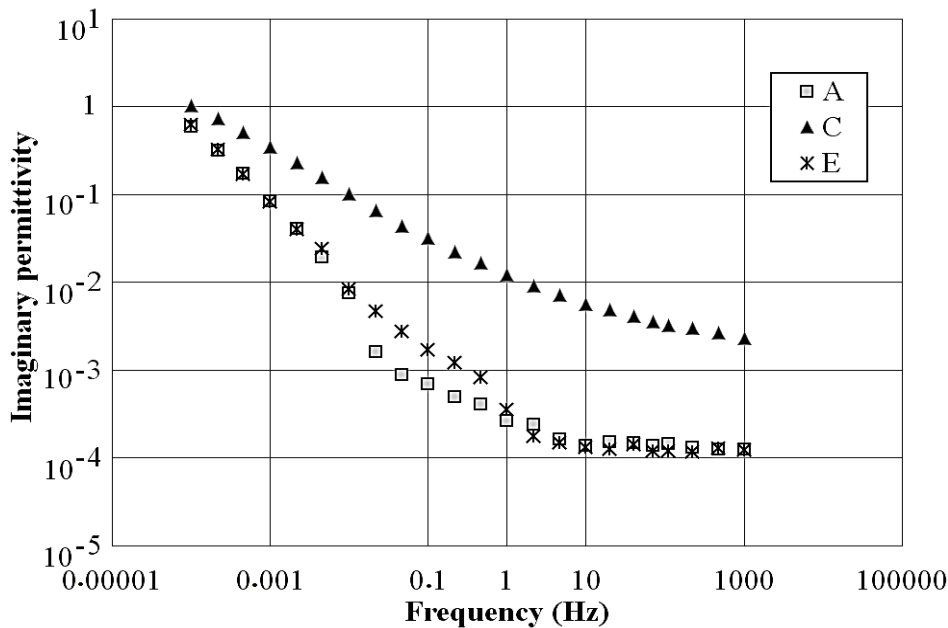


Figure 3.4. Equivalent circuit to model linear dielectrics [49, 50].

The imaginary part of the complex permittivity, which represents dielectric losses in the material, is shown in Figure 3.5b. As can be seen, its frequency dependencies for silicon rubbers A and E are almost overlapping representing similar losses in both the materials in the overall frequency window. The magnitudes of the imaginary part are higher at lower frequencies while at higher frequencies a decrease in the dielectric loss is observed. Further, for material C at high frequencies close to 1 kHz, the magnitude of the losses is in almost one order of magnitude higher as compared to the other two materials. However, at lower frequencies the absolute differences are getting smaller and at 0.1 mHz, the losses of almost the same magnitude are found in all the three materials.



(a)



(b)

Figure 3.5. Real (a) and imaginary (b) parts of the complex permittivity for different materials.

4. Charging by corona in air and surface potential decay measurements

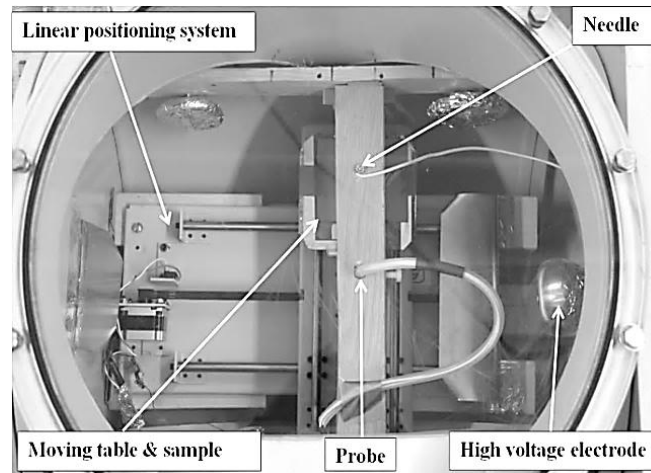
This chapter focuses on experimental setup and procedure used to deposit charges on HTV silicon rubber surfaces through corona discharges in air. The influence of different parameters like voltage amplitude, needle electrode gap distance, material properties and ambient pressure on the surface potential distribution is investigated. Potential decay measurements on pre-charged silicon rubber surfaces are performed at different pressures of ambient air in order to evaluate the contribution of gas neutralization to the total charge decay as well as to analyze solely the influence of solid materials properties on surface charge dynamics. Decay rates, field dependent bulk conductivity and distribution of trap density deduced for the studied materials from the surface potential decay characteristics are presented and discussed.

4.1 Experiments

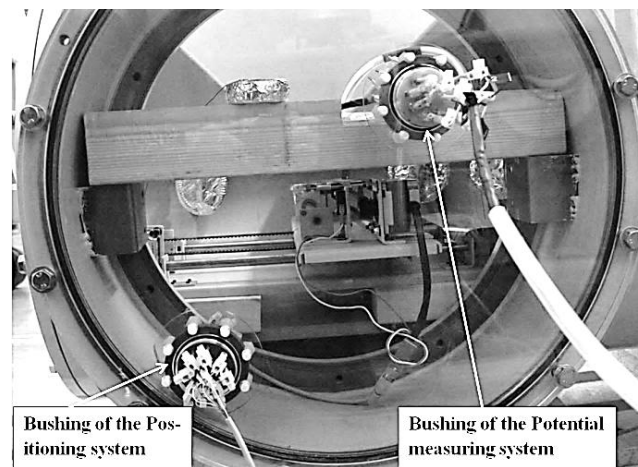
4.1.1 Experimental setup

The experimental setup was built inside a sealed metallic chamber ($\sim 1 \text{ m}^3$) shown in Figure 4.1 that allowed for carrying out the potential measurements at different gas pressures. Inside the chamber, a linear positioning system with a movable grounded table carrying a flat material sample was installed and it was connected to an external controller via a low voltage bushing. The charging arrangement included a corona needle, which was used to deposit charges onto the sample. The needle diameter was 0.89 mm with a tip radius of about 0.125 mm. The needle was mounted on a wooden arm and it was connected to an external DC voltage generator through a high-voltage bushing.

The photographs and schematic view of the charging and potential distribution measurements setups are shown in Figures 4.1 and 4.2, respectively. The surface potential measuring set-up contained a Kelvin's type vibrating probe (Trek 3455ET) installed on the same wooden arm as the corona needle and connected to an electrostatic voltmeter (Trek 341B, $\pm 20 \text{ kV}$) located outside of the chamber. The distance between the probe and the sample was fixed at about 2 mm in order to achieve accurate results. The voltmeter provided a low voltage replica (attenuated by 1000 times) of the probe potential. A voltage divider was used to further step down the potential to a ratio of 4:1 to make it possible for data acquisition system to handle it. In the tests, the positioning system was used to move the sample beneath the charging needle and the probe. Information on the position of the sample and signals from the potential probe were communicated to a computer through a data acquisition card. The pressure in the chamber was controlled by means of a rotary vacuum pump and a digital manometer (precision of 0.1%) was used for monitoring its level. The conditions in the laboratory during the experiments were practically constant (air temperature 18-20 °C, humidity $\sim 30\%$).



(a)



(b)

Figure 4.1. Top (a) and side (b) views of the sample positioning system with charging and scanning setups mounted in the test vessel. Note that the charging needle and the probe are beneath the arm and are facing downwards to the sample.

4.1.2 Experimental procedure

A material sample ($100 \text{ mm} \times 100 \text{ mm} \times L$ (thickness) mm) was placed on the grounded movable table inside the test vessel and its surface was scanned to check if the initial magnitudes of surface potential were sufficiently low (typically below 100 V). For charging, the table was brought to the position such that the tip of the needle was located at the center of the sample. Thereafter, the surface was charged by applying DC voltages to the corona needle for 2 minutes (different amplitudes and polarities were utilized). During charging, air pressure in the test vessel was equal to the external atmospheric pressure and it was evacuated down to different levels after the charging was completed. Two pressures levels, 600 ± 10 mbar and $\sim 300 \pm 10$ mbar, were considered in the present study. Immediately after the charging was completed, the needle was grounded and the table with the sample was brought to the position under the electrostatic probe which took approximately 30 sec and the surface potential measurements started. For obtaining a

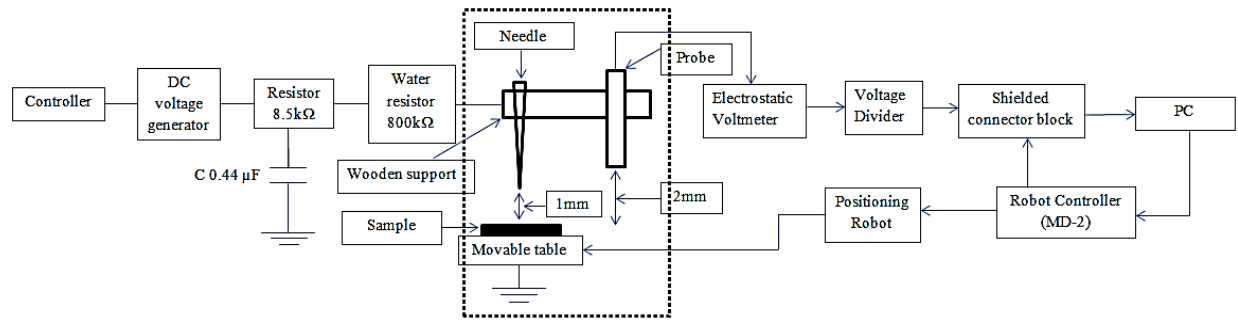


Figure 4.2. Schematic view of charging arrangement and scanning setup for surface potential distribution measurements. The broken line shows the metallic chamber wall.

distribution of the potential on the surface, the sample was moved under the probe. In the preliminary experiments, it was observed that the charging resulted in symmetrical potential distributions around the point above which the corona needle was located. For this reason, a half of a sample surface was typically scanned along a line starting from the sample edge to its center that allowed for reducing scanning time down to ~ 5 s. The measurements of the surface potentials were repeated at different instants after the charging. Between the consecutive measurements, the sample was moved to a parking position away from any sharp edges to avoid external disturbances of the surface potential.

4.1.3 Test conditions

Potential decay measurements inside the test vessel were taken at three different pressure levels that allowed for realizing the following conditions for the neutralization of deposited surface charges by air ions:

- (1) Natural gas neutralization – this condition inside the test vessel was achieved by taking the decay measurements at ambient pressure. Gas neutralization takes place due to the interaction of surface charges and free ions of opposite polarity arriving from the gas to the material surface. The free counter ions are driven by the electric field setup by the surface charges. The intensity of gas neutralization depends on the amount of ions present in the gas phase as well as on the field strength in the vicinity of the material surface.
- (2) Reduced gas neutralization – the relative contribution of gas neutralization to the total charge decay was reduced by lowering the air pressure inside the test vessel. In the present study, air pressure was reduced to a level of ~ 600 mbar due to its practical significance. From practical point of view, gas neutralization can be of primary concern for HVDC applications, where insulation system is exposed to long lasting unipolar stresses and operates under steady-state conditions defining a dynamic balance between deposition and neutralization of surface charges. This balance can be affected by external conditions, e.g., reduced air pressure due to high altitudes that appear in real life situations. Thus, HVDC power transmission lines may pass through high mountain areas, see e.g. [1] where altitudes up to ~ 4300 m are mentioned. Under such conditions, air pressure is reduced in $\sim 40\%$ as compared to normal atmospheric level. The relative contribution of the gas neutralization to the surface charge decay on insulating polymeric materials has not been investigated under such conditions.

- (3) Zero gas neutralization – refers to the situation where the potential decay take place solely due to solid material properties. This condition was achieved by measuring the decay characteristics at ~300 mbar air pressure inside the test vessel.

4.2 Determination of background densities of ions in air at different pressures

Air ion density measurements inside the test vessel are quite difficult due to the limited gas volume and a necessity to connect external devices to internal ion counters. Therefore, a feasible way is to place two sufficiently large electrodes with a certain gap inside the test vessel and to measure the ion current using e.g. Keithley 6517A electrometer as a response to the applied voltage. The obtained current values at different air pressures can be post-processed to deduce the required parameters. However, it is important to mention here that Keithley device cannot measure a current lower than 0.1 pA due to its sensitivity level. Therefore, measuring current in the linear region of voltage-current characteristics of air [17] in the present setup is not possible. Therefore, the only possibility is to measure current in the initial phase of an exponential region of the characteristics. The developed experimental setup and procedure are described as well as obtained results are presented below.

Experimental setup and procedure

Special experiments were conducted inside the test vessel to evaluate the effect of air pressure on the background density of free ions in gas phase. The experimental setup consists of a pair of electrodes of Rogowski shape (diameter 100 mm, gap distance 8.5 mm) shown in Figure 4.3 placed inside the metallic test chamber. The top electrode was connected to the external HVDC generator through a high-voltage bushing while the lower electrode was connected to Kiethely electrometer 6517A via dedicated bushing.

The background ion density was deduced from the current voltage characteristics obtained at different pressures of ambient air. First, the pressure inside the test chamber was reduced down to a certain level using vacuum pump and then the voltage, significantly lower than the breakdown threshold, was applied to the top electrode. The voltage was increased in steps and the corresponding current was recorded. At each increase in voltage step there was a hike observed in

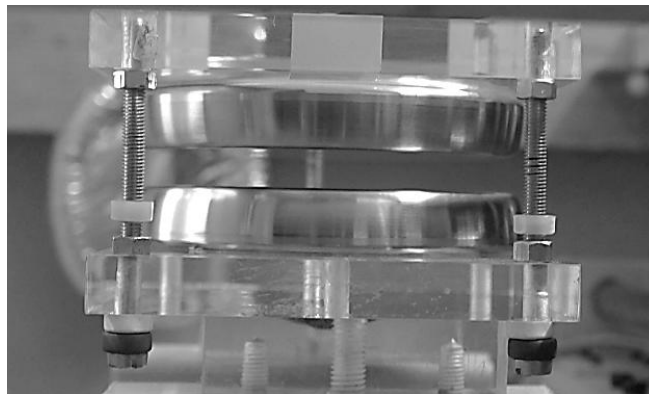


Figure 4.3. Rogowski shaped electrodes for ion current measurement inside the test vessel.

the current due to polarization and, therefore, the current was allowed to relax to a constant value before the next voltage step was applied. The same procedure was repeated at different air pressures.

Ion current measurement at different air pressures

The measured currents are shown in Figure 4.4. As can be seen, the slope of the lines gets steeper with the drop in the pressure level. Also, the experimentally obtained current at a particular applied voltage have lower values at reduced air pressures, though the electric field (reduced electric field) is much higher. The ion density is calculated from the data points using the current density equation

$$J = q\mu nE \quad (4.1)$$

Here, q is the elementary charge, μ is the average mobility set to $2 \text{ cm}^2/\text{Vs}$ [52], n is the concentration of charge carriers and E is the electric field. The calculated n values using equation 4.1 are shown in Figure 4.5 as functions of the reduced electric field. As seen, the densities of the charge carriers tend to increase when the applied field becomes stronger that corresponds to the initiation and intensification of electron impact ionization in air, i.e., to the appearance of Townsend's discharge. This process can be mathematically represented as

$$n = n_0 e^{\alpha d} \quad (4.2)$$

Here, n_0 is the background ion density, α is the Townsend first ionization coefficient, and d is the

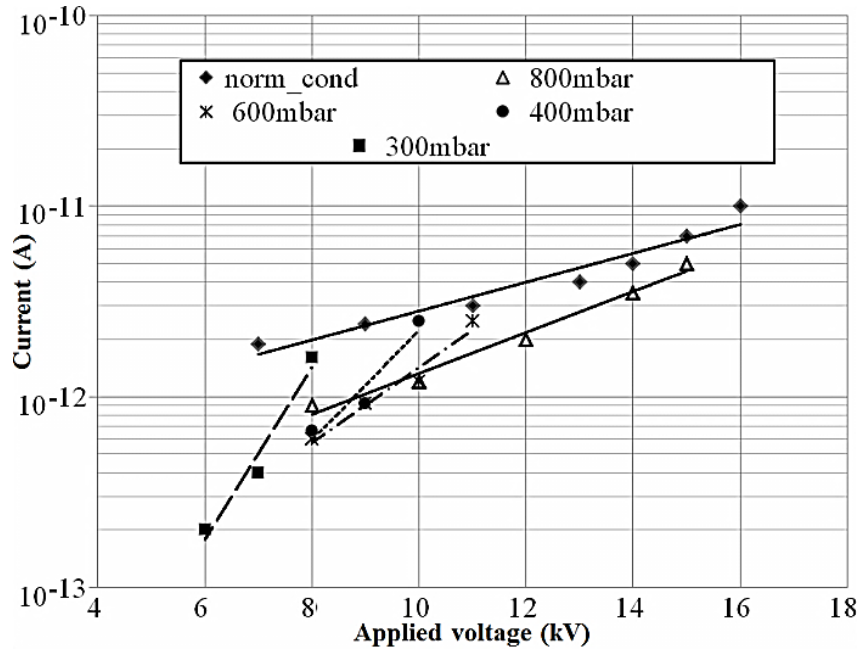


Figure 4.4. Ion current measured at different air pressures. The solid and broken lines are the exponential fitting of the experimental points.

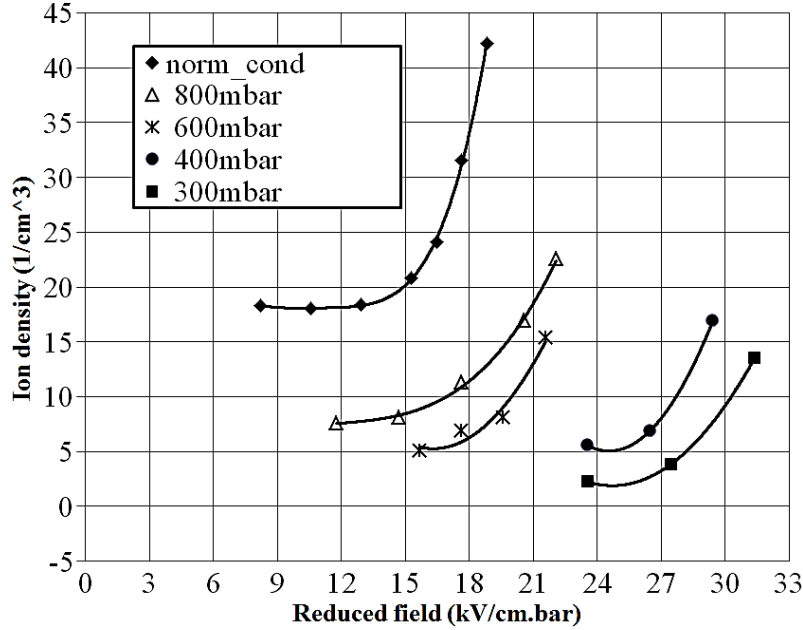


Figure 4.5. Ion density measured inside the test vessel at different ambient pressures. The solid lines are the fitting of the experimental points.

gap distance between the two electrodes. In principle, equation (4.2) can be used for obtaining n_0 provided that the dependence of α on field strength is well defined. The results of such calculations are shown in Figure 4.5. As follows from the curves, their leftmost points corresponding to the lowest field strength in the experiments yield magnitudes of the background ions density n_0 . One can observe that the measured concentration at normal pressure is $\sim 20 \text{ cm}^{-3}$ that is well below of the commonly accepted values $\sim 10^3 \text{ cm}^{-3}$ [53] for open air. Such significant difference can be attributed to a screening effect of the grounded metallic vessel which attenuates the intensity of external factors (terrestrial radiation, cosmic rays) responsible for the background ionization of the gas. The reduction of the pressure down to 300 mbar yielded a significant drop (~ 10 times) of the ions density, which can be related to the decrease of the gas concentration, i.e. the number of molecules available for ionization. Hence, the amount of ions which may contribute to surface charge relaxation/decay is negligible under such conditions and thus, charge dynamics can be solely considered due to solid material properties.

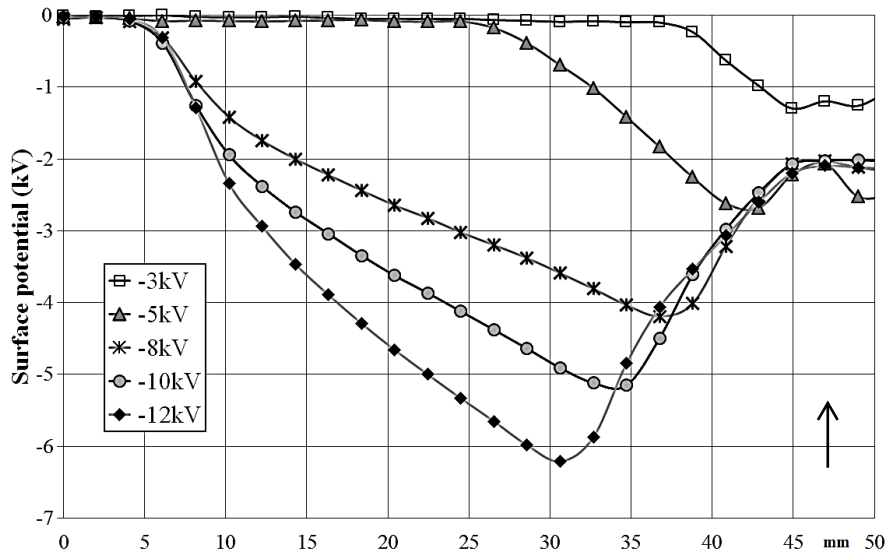
4.3 Surface charging under different conditions

The preliminary experiments were performed on material B to investigate the effect of voltage magnitude and distance of the needle electrode to the surface on resulting potential distributions. The obtained potential profiles are discussed in the following sections.

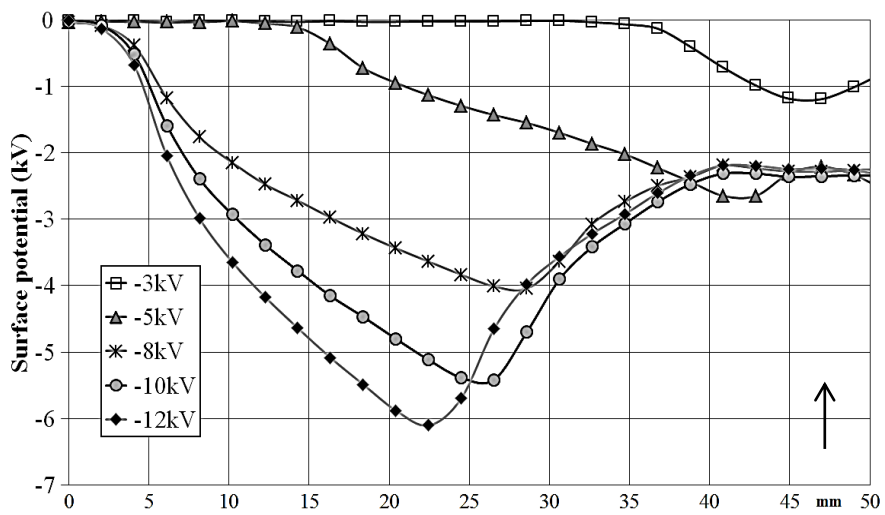
4.3.1 Effect of charging voltage magnitude

Surface potential distributions obtained with different amplitudes of the negative dc charging voltages at distances of 1 mm and 3 mm between the needle tip and the material surface are shown in Figure 4.6a and Figure 4.6b, respectively. Potential distributions are obtained only for a half of the sample due to symmetrical charging. A complete profile can be obtained by mirroring

the distributions around the central point. As can be seen, for 1 mm gap distance, all the potential distributions are characterized by a maximum magnitude that increases from $\sim -1.3\text{kV}$ to $\sim -6\text{kV}$ appearing at a distances of 30 – 45 mm from the edge of the sample. The maximum values of the surface potential move towards the zero co-ordinate with the increase in the amplitude of the applied voltage and, therefore, cause an increase in the area covered by the charge spot. Further, it can be noticed that all the potential distributions are saddle shaped, which have been observed in other studies, see e.g. [6, 54]. For -3kV , the saddle shape is weaker and the area of the charge spot is smaller, however, the difference between the maxima and the minima of the potential becomes stronger and the size of charge spot increases at the voltage amplitude -12kV . The



(a)



(b)

Figure 4.6. Surface potential distributions obtained with different amplitudes of the negative dc charging voltages at needle electrode to surface gap distances of 1 mm (a) and 3 mm (b). The arrow indicates the location of the corona needle during charging (the center of the sample).

saddle shape is claimed to occur most probably due to back discharges compensating overcharging of the surface immediately after switching off the corona voltage and grounding the corona electrode. For all the applied voltages except -3kV, the potential profiles at the location of needle are minimized to a voltage level of ~ -2 kV due to neutralization caused by the back discharges. The neutralized area is defined under the curve between the maximum magnitude of surface potential and central point where the corona needle is placed. Since, with the increasing charge spot, the area covered by the electric field lines is getting larger, therefore, causing an increase in the intensity of back discharges.

For needle electrode gap distance of 3 mm, similar potential distributions as that for 1 mm gap distance are obtained. However, an increase in the area of the charge spot and spread in the surface potential is observed as compared to the previous case,. For the voltage of -3 kV, the potential distribution is bell shaped, however, the profile is transformed into saddle shape at -5 kV and it becomes even more prominent as the corona voltage approaches -12 kV. Also, it can be noticed that with the increasing gap distance the back discharges become more intense and, therefore, causes an increase in the neutralization area.

From the above demonstrations one may suggest that increasing either of the two parameters (voltage amplitude or needle electrode gap distance) will result in a larger area of charge spot and more spread of the surface potential.

It important to mention here that in the rest of the study, voltage amplitudes of ± 12 kV and needle electrode gap distance of 3 mm is used to charge the material surface.

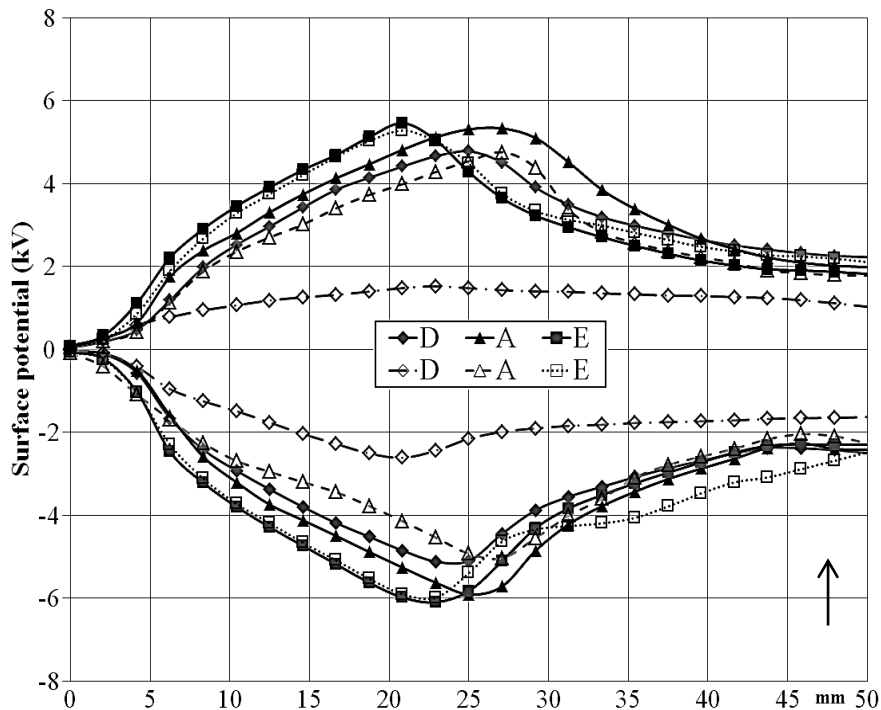


Figure 4.7. Measured surface potential profiles. Solid lines are distributions obtained at atmospheric pressure at 30 s after charging. Broken lines show the profiles recorded at 300 mbar and at 3 min after charging (immediately after completing gas evacuation).

4.3.2 Effect of materials properties

Potential distributions measured on HTV silicon rubber samples at two different pressures of ambient air after charging are shown in Figure 4.7. As it is seen, all the obtained profiles are characterized by a maximum magnitude appearing at distances 20-30 mm from the edge of the sample and reduced potentials at the center of the sample. Despite of the non-uniform surface charging, the obtained potential profiles allow for establishing some regularities. Thus, it can be observed that the distributions for both polarities of the charging voltage have in general similar shapes. However, the magnitudes of the surface potential at negative polarity are slightly higher. This reflects larger amount of negative charges which are accumulated on sample surface. Furthermore, the potential distributions obtained at atmospheric pressure (solid lines) demonstrate that surfaces of the materials used could be charged in different ways and up to different levels depending upon their properties. Thus, one may notice a correlation between the materials parameters provided in Table 3.2 and the surface potential distributions – the lower are the surface and bulk conductivity values, the larger is the size of the charged spot on the surface and the higher is the peak value of the potential. The effect of the material is found to be even more pronounced at 300 mbar air pressure (broken lines). Thus, the reduction of the surface potential as compared to its magnitudes at normal pressure is more significant for more conductive materials. One should note, however, that the potential drop that occurred during the evacuation process, which lasted ~3 min, depended also on the initial conditions, in particular on the amount of deposited charges (and thus the induced surface potential) at normal pressure. Potential distributions measured at 300 mbar are used as initial conditions to run the simulation model which is discussed in chapter 5.

4.3.3 Effect of ambient air pressure

In order to evaluate the effect of pressure level on surface charging, air pressure inside the test

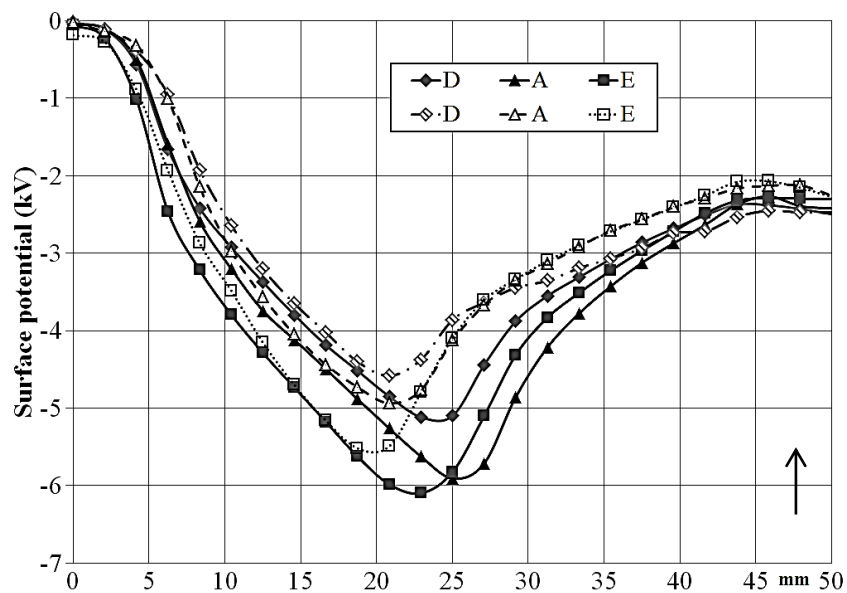


Figure 4.8. Surface charging at two different pressures of ambient air. Solid and broken lines are potential distributions obtained 30 s after charging at atmospheric and at ~600mbar pressure respectively.

vessel was reduced down to ~600 mbar. Surfaces of different types of HTV silicon rubbers were charged and potential distributions obtained immediately after charging are shown in Figure 4.8. For comparison purpose, potential distributions measured on the same materials at normal air pressure are also shown in the figure. As can be seen, potential profiles for each material sample at two different air pressures are very similar in shapes. However, there is a decrease in the maximum magnitude of surface potential obtained at ~600 mbar as compared to that at atmospheric pressure, which can be attributed to either of the two reasons.

- (1) The voltage applied to the corona needle causes the ions present in the gas phase to set on the material surface and contribute to surface charging [55]. Therefore, a decrease in the maximum magnitude of surface potential indicates the fact that the amount of gas ions get lower as the pressure inside the test vessel is reduced.
- (2) The back discharge phenomenon, which causes neutralization of the surface potential after switching off the corona and grounding the corona electrode, can be intensified due to decrease in the pressure level. Therefore, the neutralization area is larger as compared to the case of ambient pressure and, as a consequence, the peak surface potential is reduced.

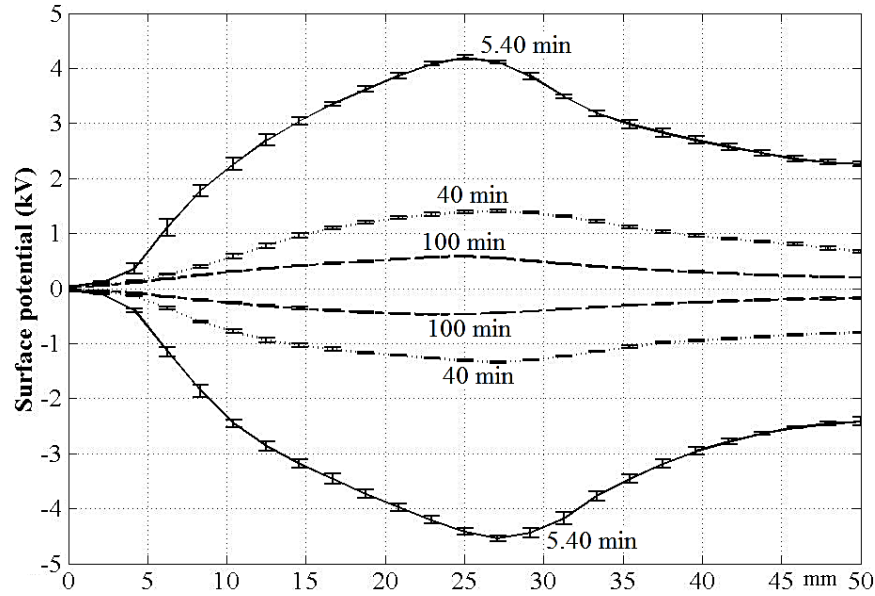
4.4 Surface potential decay

Surface potential decay on pre-charged silicon rubber surfaces was recorded at different pressures of ambient air. The effects of various parameters such as amount of ions present in the gas phase, polarity of deposited surface charges and influence of solid materials properties on surface charge dynamics were investigated. Depending on the material properties and pressure level inside the test vessel, decay measurements took a time span of couple of minutes to couple of weeks. The obtained surface potential decay characteristics are described in the following sections.

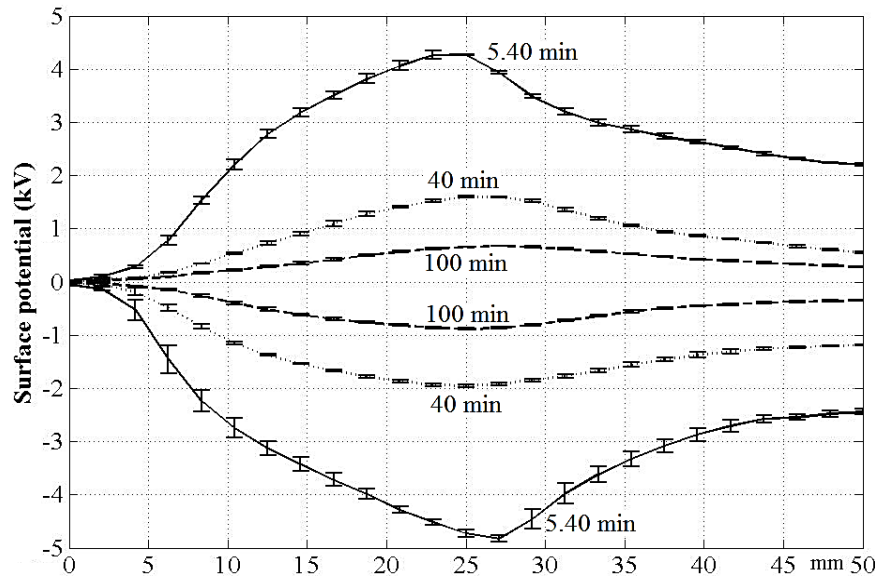
4.4.1 Potential decay at different pressures of ambient air

Surface potential distributions measured at two ambient pressures for materials C and E are shown in Figure 4.9 and Figure 4.10 respectively. It is worth to mention that each experiment under similar conditions was conducted three times. The recorded potential magnitudes at different locations on the material surface were post-processed to get meaningful values. The obtained parameters in both the figures are shown by error bars that represent standard deviations while the mean values are connected by lines and represent potential distributions. As can be seen, deviations from the mean surface potential at different time instant during the decay process is not significant indicating that measurements have good repeatability.

As seen, potential profiles measured at different instants during the decay process doesn't show the lateral spread of the charged spot on the material surface indicating that contribution from surface conduction to the charge decay is insignificant. Furthermore, comparing the potential distributions at both the ambient pressures indicate that the decay process takes longer time at reduced air pressure. The latter effect is due to the fact that contribution of free ions to neutralization of the surface charges diminishes with the reduction of the gas pressure in the test vessel as was shown in section 4.2 above. The weak effects of both the surface leakage and gas neutralization suggest that bulk conduction is the most probable mechanism affecting potential decay. This may also be observed from the potential profiles, magnitudes of which are decreasing with time without significant modifications in distributions' shapes.



(a)

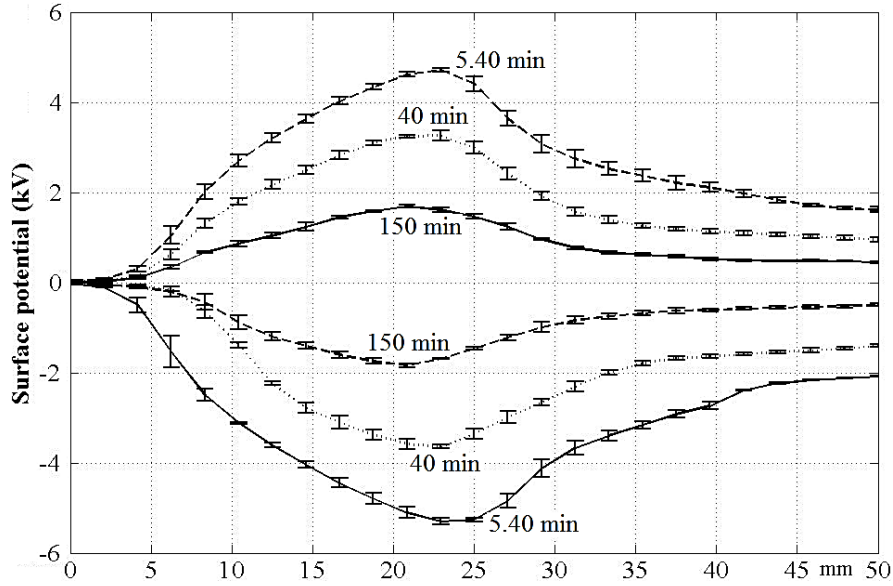


(b)

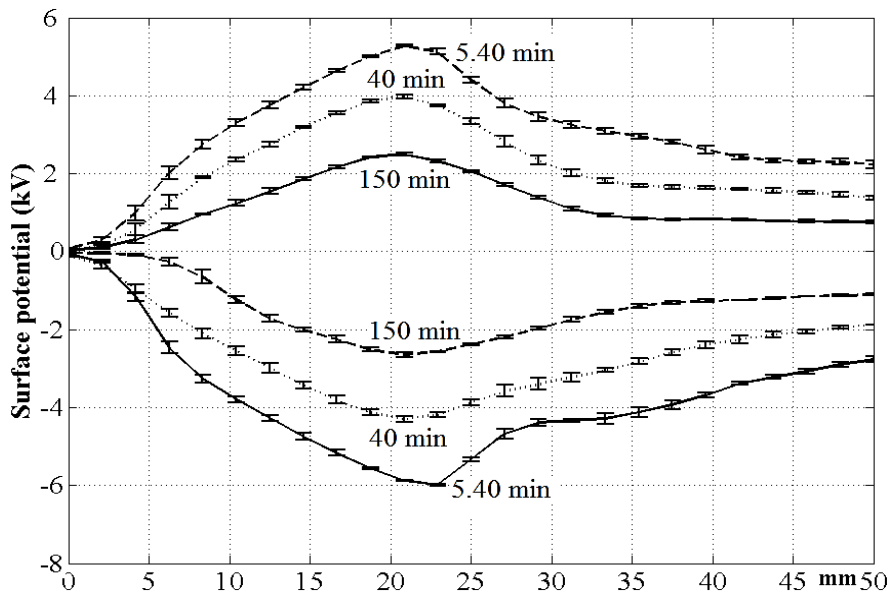
Figure 4.9. Measured surface potential distributions at different time instants during the decay process on material C at normal (a) and 300 mbar (b) air pressure.

Decay of the maximum magnitude of surface potential

The non-uniformity of the measured distributions (arising due to the charging method used) allowed for obtaining potential decay characteristics at different locations on sample's surfaces, i.e., at its different initial magnitudes and thus induced fields in the material. Normalized surface potential decay characteristics obtained for the locations corresponding to the maximum values of V_s on samples of different materials are shown in Figure 4.11. As can be seen, the decay process is strongly affected by the material properties. Thus, the time needed for the reduction of the



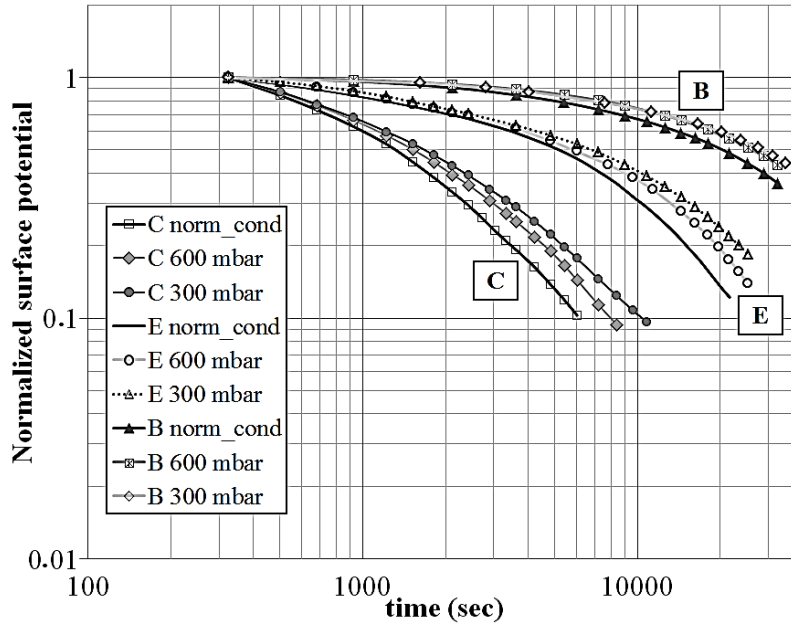
(a)



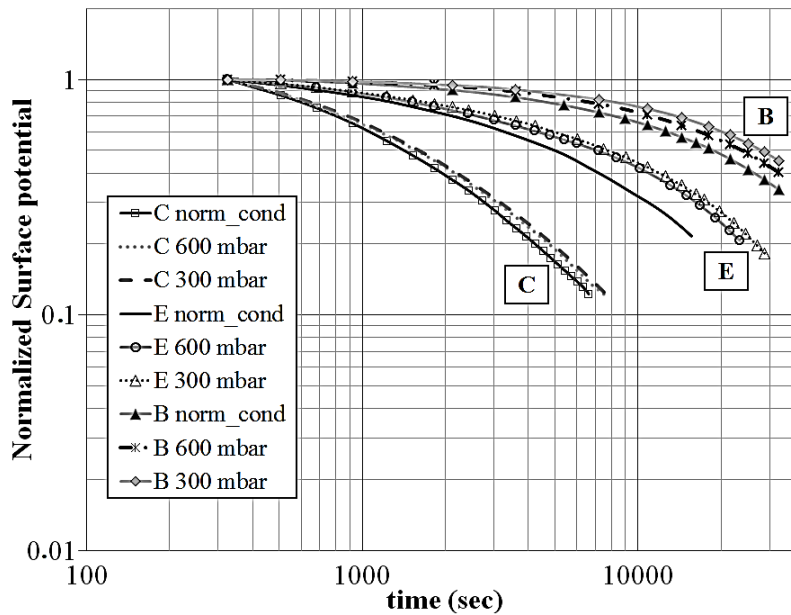
(b)

Figure 4.10. Measured surface potential distribution at different time instants during the decay process on material E at normal (a) and 300 mbar (b) air pressure.

potential down to 50% of its initial value is the shortest for material C, it is approximately four times longer for material E and in more than ten times longer for material B. This correlates well with the measured bulk and surface conductivities of the materials (Table 3.2). As seen, the fastest decay is for the relatively most conductive material (C) while the slowest is for the most resistive one (B). The polarity of the deposited charges does not seem to affect the decay process significantly (compare corresponding curves in Figure 4.11a and 4.11b).



(a)



(b)

Figure 4.11. Surface potential decay characteristics for different materials at different air pressures for (a) negative and (b) positive charging. The surface potential is normalized to its maximum value corresponding to the first measured point.

As seen from Figure 4.11, the potential decay becomes slower at the reduced pressure levels for all the materials and both polarities of deposited surface charges. Further, one can also observe that the potential decays faster at the beginning of the process when its magnitudes are relatively high. This is clearly seen in Figure 4.12 where the decay rates, dV_s/dt , deduced from the measured characteristics are presented. At higher magnitudes of surface potential, higher amount

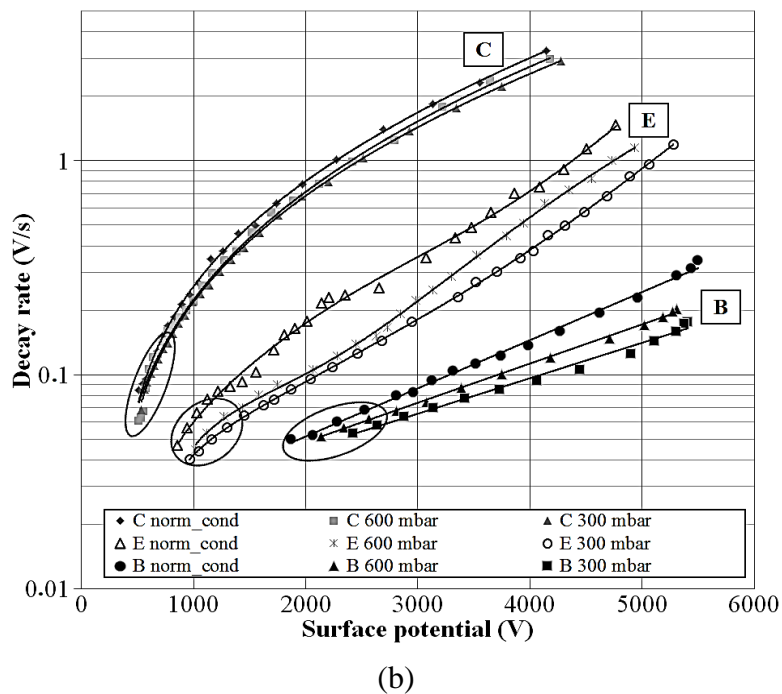
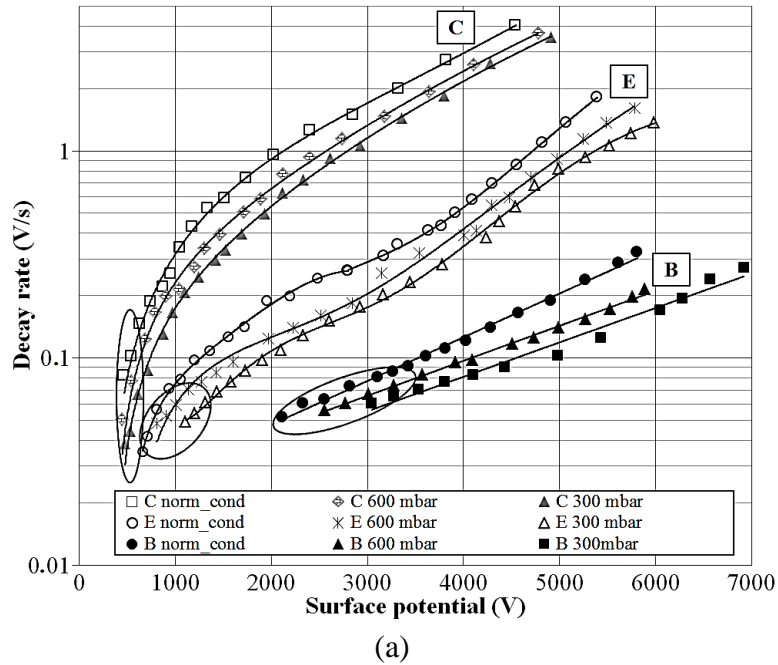


Figure 4.12. Decay rates of surface potentials at (a) negative and (b) positive charging for different materials and gas pressures. The solid lines represent the results of fitting.

of surface charges can induce stronger electric fields within the gas volume thus making the arrival of counter ions present in air and neutralization of the deposited charges more efficient. At lower potential magnitudes, the decay rates decrease and tend to merge into the same region (encircled areas). In addition to that, for the studied materials, the effect of the gas pressure and, hence, gas neutralization on decay rates can be clearly observed in Figure 4.12. As seen, the reduction of pressure yields to smaller decay rates without bringing a major change in the shapes

of the characteristics. The relative differences between the decay rates at different air pressures are similar for all materials. The exception is the set of data for material B at positive polarity (Figure 4.12b) where one can observe just small deviations due to the change in gas pressure. The reason for this is unclear and requires further analysis.

The demonstrated influence of the reduction of gas pressure on surface charge dynamics can be explained by lower amount of free ions present in air at its reduced density, which are available due to background ionization processes in the gas phase [53]. In order to validate this, special experiments were conducted inside the test vessel as was described in section 4.2.

4.4.2 Influence of material properties

In order to solely analyze the role of solid material properties (conduction mechanisms and polarization processes) on surface charge dynamics, normalized surface potential decay characteristics obtained for the locations corresponding to the maximum values of V_s measured at 300 mbar ambient pressure on samples of different materials are shown in Figure 4.13 (a and b) by solid lines. As seen, the material plays a deterministic role in the decay process. Thus, time to drop to 50% value is ~50 times longer for material B than for material D. Moreover, mechanisms governing surface potential/charge dynamics seem to be different. As it is known [16, 28], exponential character of the decay is typically associated with intrinsic conduction process while other mechanisms (charge injection, slow polarization, etc.) result in power law type dependences. For the studied materials, the decay characteristics are better fitted by exponential functions (Figure 4.13a), either completely (materials B and E) or partially (materials A, C and D), rather than by a power law (Figure 4.13b). The latter, however, appears to be suitable for describing the surface potential decay for material D (compare the fits in Figures 4.13a and 4.13b). Based on these observations, one may suggest that conduction is mainly responsible for the surface potential/charge decay in most of the studied materials. The fitting parameters are provided in Table 4.1.

Table 4.1. Parameters used for fitting surface potential decay characteristics measured for HTV silicon rubber samples.

Materials	a·exp(b·t)		c·t ^d	
	a	b	c	d
D	1.824	- 0.002	561.3	- 1.093
C	0.985	- 0.0004	25.56	- 0.544
A	0.929	- 0.0002	8.722	- 0.357
E	0.916	- 0.00007	6.82	- 0.307
B	0.974	- 0.00002	2.691	- 0.151

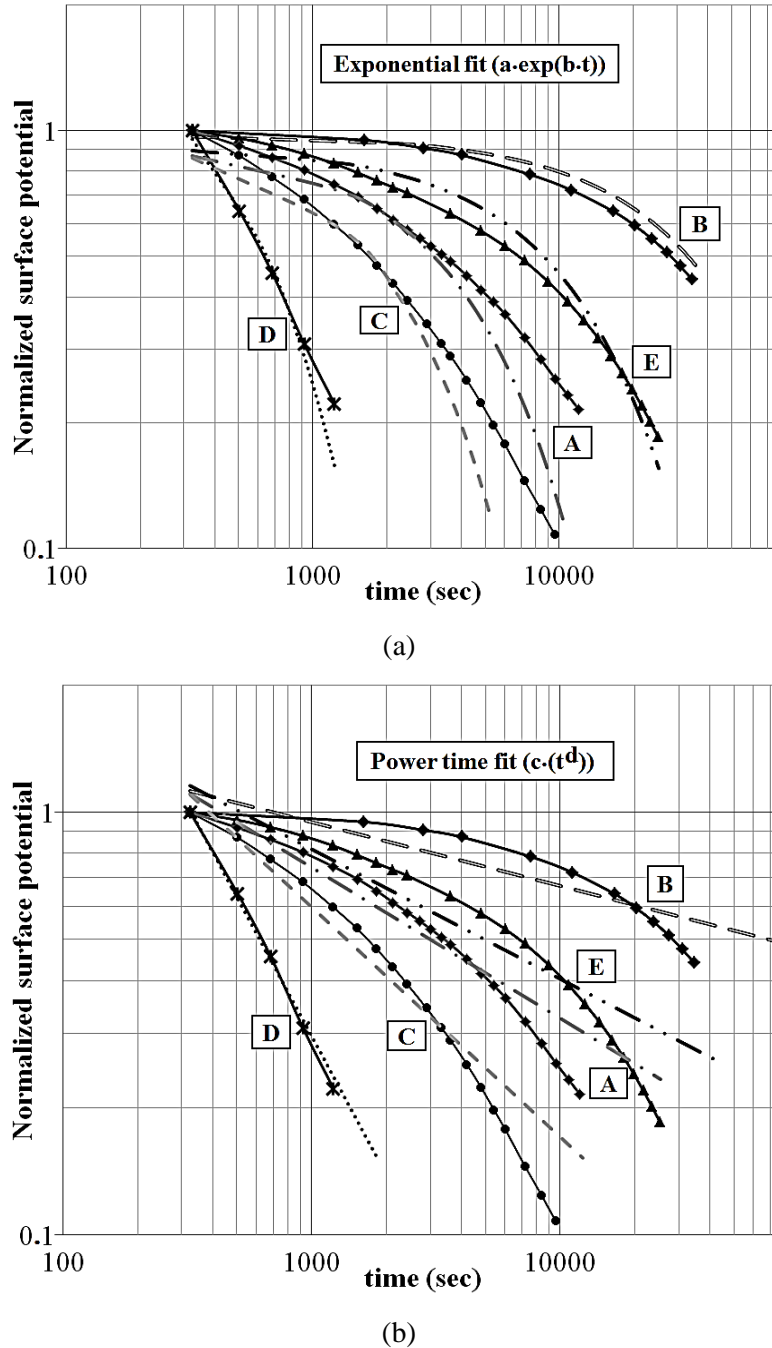


Figure 4.13. Surface potential decay characteristics fitted with (a) exponential and (b) power laws. The solid lines with markers represent the experimental data while the dotted lines show the fits.

The rates of potential decay for the studied material samples were calculated from the measured surface potential characteristics and are shown in Figure 4.14 (maximum values of V_s were used). As can be seen, the decay rate increases with increasing magnitudes of V_s for all the materials that suggests an enhanced conduction in the bulk due to stronger internal fields induced by higher surface potentials. However, the characters of the variations are different for different materials as well as for the polarity of surface potential. Thus, the decay rate obtained for material D

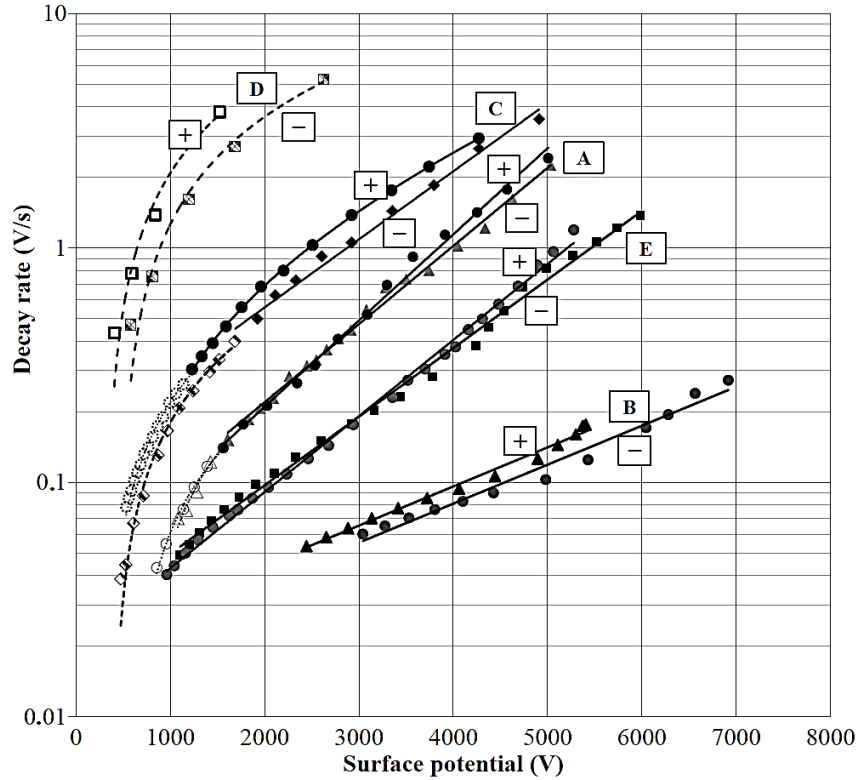


Figure 4.14. Surface potential decay rates for different materials calculated from the maximum V_s values measured at 300 mbar, solid lines represent the regions with exponential behavior while dotted lines indicate regions with linear variations.

increases practically linearly with V_s while an exponential behavior is observed for E and B materials (note the logarithmic scale in the figure). For rubbers A and C, both regions exist and the transition point appears to be at $V_s \sim 1.7$ kV for negative surface potential and at $V_s \sim 1.3$ kV for positive surface potential. These features cannot be explained based on the fixed conductivity values obtained from the standard tests given in Table 3.2.

4.5 Evaluation of materials properties from potential decay characteristics

Measurement of surface potential decay is a powerful tool to characterize insulating materials and charge transport mechanisms. As mentioned above, potential decay under normal conditions is generally accepted to be due to contribution of three mechanisms: bulk and surface conduction as well as gas neutralization. In the present study, due to specially created experimental conditions as discussed in section 4.2, the intensity of gas neutralization to the total charge decay is minimized. Also, due to the absence of lateral spreading of surface charges during the decay process, as shown in Figure 4.9 and Figure 4.10, it can be suggested that surface conduction plays minor role. Hence, one may assume that intrinsic conduction is mainly responsible for surface potential kinetics. Complementing such model with an assumption about partial injection of charges into surface layers, it is possible to deduce certain material properties, such as field

dependent bulk conductivity and energy distribution of trap states, from the experimentally obtained potential decay characteristics.

4.5.1 Field dependent bulk conductivities

Field dependent materials conductivities are typically obtained from standard measurements (as described above in section 3.2) performed at different test voltages. To realize this, a sample is placed between two metallic electrodes with fixed potentials and a current through the material is recorded. Alternatively, results of surface potential decay measurements can be utilized provided that potential magnitudes at each instant correspond to voltages applied across a material sample induced by deposited surface charges (this is the situation in the present experiments where one side of the sample was always grounded during the measurements). It is worth mentioning that this approach yields a dynamic apparent conductivity (due to the decaying potential) that may differ from equilibrium value. The latter can be, in principle, obtained from standard voltage-current measurements at sufficiently long times (which may reach $\sim 10^5$ s for the studied materials) required for mitigating capacitive current component through the sample. In practice, however, such long-lasting measurements are not feasible and are usually interrupted when it is decided that the capacitive current is sufficiently low thus resulting in conductivity values which may (or may not) be close to equilibrium magnitudes. Hence, both approaches are characterized by some uncertainties in the results. However, the method based on surface potential decay may be preferable for obtaining field dependent conductivities due to the fact that the potential decay

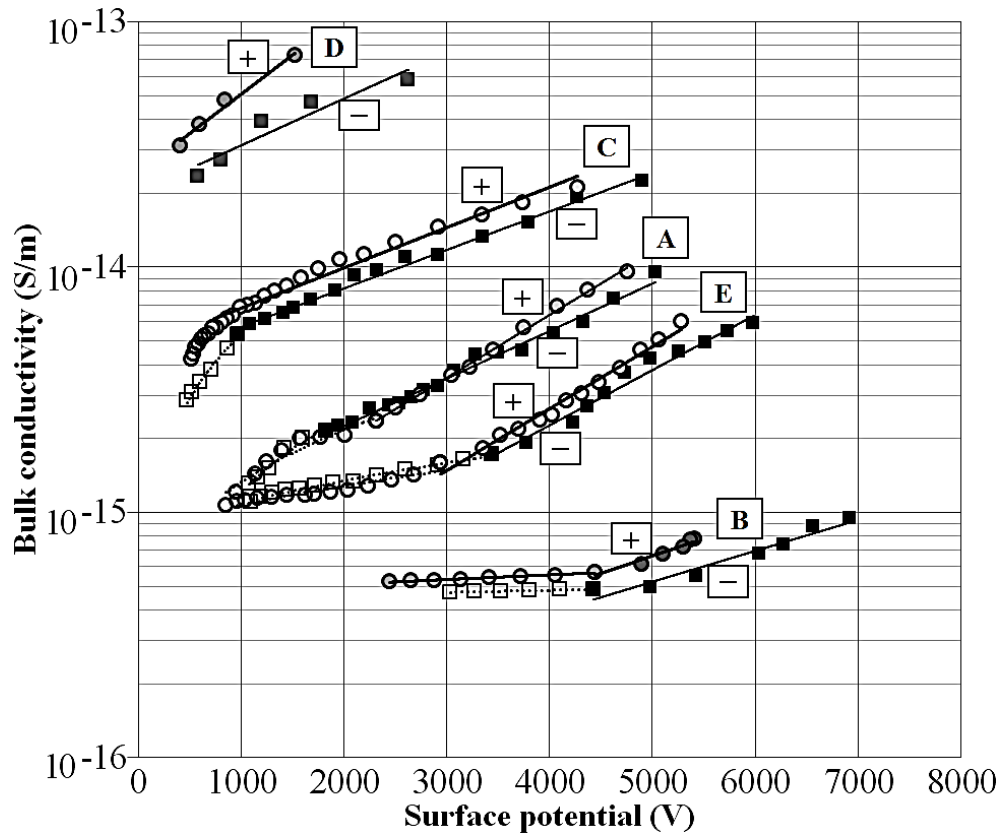


Figure 4.15. Field dependent bulk conductivities deduced from the measured surface potentials, filled markers fitted by solid lines represent the exponential part of the dependence while empty markers fitted with dotted lines are for the linear part.

is a natural process controlled only by properties of the material and surrounding gas. Under conditions of the present study, the influence of the latter is minimized and the effect of surface conduction can be neglected as discussed above. Therefore, field dependent bulk conductivities of the studied materials deduced from the data in Figure 4.14 utilizing the model (2.5) - (2.7) are shown in Figure 4.15 as functions of V_s . As it is seen, the obtained conductivity values increase with increasing surface potential. For all the materials, a region with practically linear increase at relatively low values of V_s is followed by an exponential rise at higher values (fitted by the solid lines in the semi- logarithmic scale used). The magnitude of V_s corresponding to the transition is different for different materials, but it is lower for higher overall conductivity values. Thus for material D with the bulk conductivity greater than $\sim 10^{-14}$ S/m, the non-linearity is of exponential type even for surface potentials as low as ~ 600 V. For material B, the conductivity is below $\sim 10^{-15}$ S/m and the linear dependence at low potential magnitudes turns into a region with practically constant magnitude $\sim 5 \cdot 10^{-16}$ S/m.

The dependences of the conductivities on surface potential may occur due to field-assisted transport of charged species through the material associated with different physical processes, e.g., charge trapping and de-trapping, ionization of impurities resulting in ionic conduction, space charge accumulation, etc. Such mechanisms can be activated if the field strength within a material induced by deposited surface charges becomes strong enough [36, 47, 56] or even at relatively low fields if, e.g., charge trapping is concerned. If expression (2.6) is used to represent field dependent conductivity, an overall effect of these processes is to be reflected by the exponential factor β . Thus, its smaller values indicate weak exponential behavior of the bulk conductivity (zero limit corresponds to a constant conductivity) and vice versa for higher values of β . The parameters in (2.6) calculated for the studied materials by fitting the exponential branches in Figure 4.15 are shown in Table 4.2. As seen, for negative surface potential, the smallest factor is found for material B and the strongest exponential dependence is observed for material E for which β is ~ 2.6 times higher. Such large discrepancies can be related to the fact that different material specific physical processes (among those mentioned above) can be intensified in stronger fields induced by higher surface potentials. This may also be the reason for the deviations of the experimental values of β from the theoretical ones seen in Table 4.2 for materials A, B and E. At the same time for silicon rubbers D and C the agreement is quite reasonable regardless of the polarity of surface potential indicating that their field dependent conductivities obey Poole-Frenkel model. In general, the levels of the conductivities and values of β obtained from the surface potential decay characteristics are of the same order of magnitude as the values obtained from standard measurements and using equation (2.7) respectively.

The field dependent bulk conductivity of the studied polymers can be attributed to intrinsic parameters defining the charge transport process, in particular, to the apparent mobility of charge carriers and the density of bulk traps. The magnitudes of the mobilities estimated from the expression $(dV_s/dt)_{t=0} = 0.5\mu(V_s/L)_{t=0}^2$ [57] using the initial (highest) magnitudes of V_s and corresponding decay rates from Figure 4.14 are shown in Table 4.3. As seen, there is a direct correlation between the obtained values of μ for different materials and their conductivities (larger magnitude of mobility provides higher conductivity).

Table 4.2. Parameters of Poole-Frenkel model and materials conductivities obtained with different methods (the value marked with * is obtained by extrapolation).

Parameter	Material				
	D -/+	C -/+	A -/+	E -/+	B -/+
K_v , fS/m, from standard test at 1kV	85.0	5.44	3.72	3.55	1.0
K_v , fS/m, from potential decay at 1kV	32.0/50.0	6.0/7.0	1.3/ 1.3	1.1/ 1.1	~0.5*
K_{v0} , fS/m	10.8/12.9	2.0/2.43	0.28/0.08	0.022/0.047	0.081/0.02
β experimental $\times 10^{-2}$	3.85/4.43	3.53/ 3.29	4.72/6.76	7.27/6.48	2.86/4.87
β from (2.7) $\times 10^{-2}$	3.55	3.30	3.99	3.59	4.0

As it was already mentioned above with regards to Figure 4.13, the intrinsic conduction of studied materials is the dominant mechanism of potential decay. Therefore, it implicates that field dependent bulk conductivity of the insulating materials should only be a function of magnitude of surface potential rather than the radial position of the material surface. In other words, if different locations on the material surfaces that correspond to different initial voltages are selected, the curves of the calculated bulk conductivities must overlap. In order to validate this fact, the magnitudes of the conductivity of materials A and E deduced from the potential decay rates obtained at different locations on samples surfaces are shown in the Figure 4.16. Note that the conductivities are presented as functions of $V_s^{1/2}$ following equation (2.6). As can be seen, the deviations of the data are not significant for both the materials and the conductivity values increases with increasing magnitude of surface potential. However, the effect of the field is quite weak and it results in just small variations of the conductivities which are within one order of magnitude or even less. Therefore, in the present study, injection of air ions into the polymer followed by their drift/diffusion in the bulk is considered as the process which has no physical significance at low energies of the charged species provided by the charging method used. The described conductivity profiles also confirm the hypothesis, developed on the basis of experimental measurements of surface potential decay and described in section 4.4.2.

Table 4.3. Apparent mobilities deduced from surface potential decay characteristics.

Material	D -/+	C -/+	A -/+	E -/+	B -/+
μ , m^2/Vs	$6.1 \times 10^{-12} /$ 1.4×10^{-11}	$1.1 \times 10^{-12} /$ 2.7×10^{-12}	$6.5 \times 10^{-13} /$ 1.5×10^{-12}	$3.3 \times 10^{-13} /$ 5.3×10^{-13}	$4.5 \times 10^{-14} /$ 4.8×10^{-14}

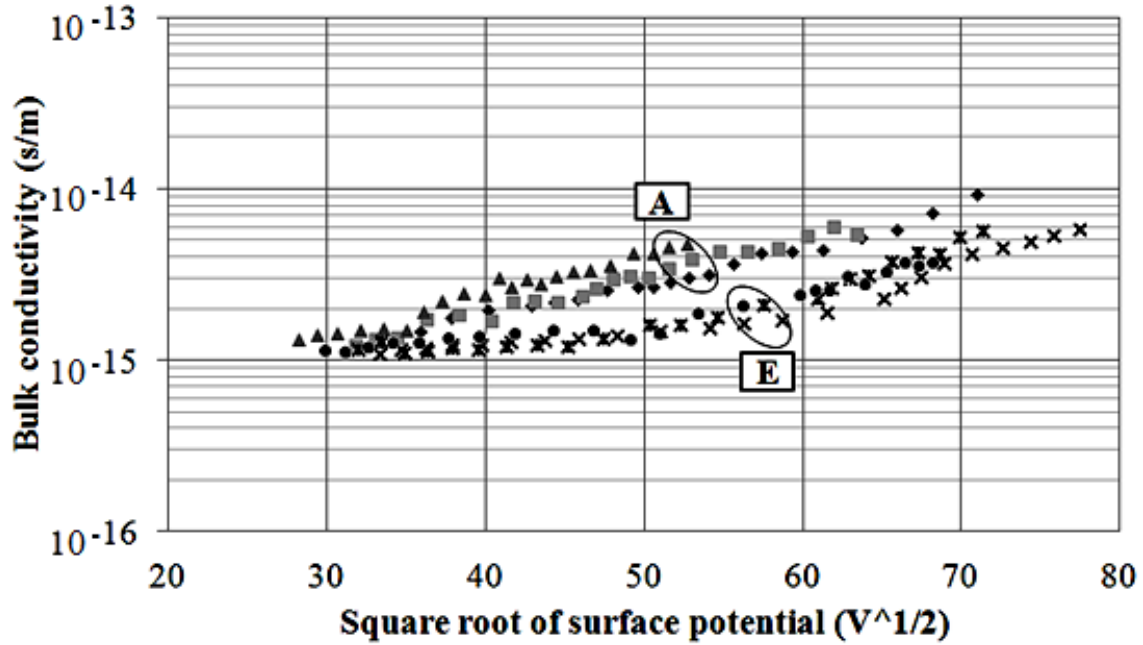


Figure 4.16. Conductivities of materials A and E deduced from the surface potentials measured at three different locations on the sample separated on a distance of 5mm from each other.

Deviations in the field dependent conductivity values, calculated at different points, are observed for certain other materials where field strengths induced by the deposited surface charges are much higher compare to the present case [58]. Such discrepancies are attributed to the fact that space charge effects or charge injection into the material bulk may no longer be ignored and, consequently, intrinsic conductivity cannot be considered as a major parameter to fully describe the charge dynamics.

4.5.2 Trap density distributions

The energy distributions of the densities of the bulk traps in the studied materials can be related to the measured decay rates as [59 - 62]

$$J(t) = \frac{\epsilon_r \epsilon_0}{L} \frac{dV_s}{dt} \quad (4.3)$$

$$J(t) = \frac{qLkT}{2t} f_o(E_t) N_t(E_t) \quad (4.4)$$

$$E_t = KT \ln(\gamma t) \quad (4.5)$$

Here, J is the current density, ϵ_0 is permittivity of vacuum, ϵ_r is the relative permittivity of the material, t is time, E_t is the trap energy, γ is the attempt to escape frequency of electrons in traps (set to $10^{12} s^{-1}$), q is the electronic charge, L is the sample thickness and $f_o(E_t)$ is the initial occupation probability of traps (set to $1/2$).

It is important to mention here that decay is solely considered due to intrinsic conduction associated with partial injection in charged surface layers and all the other mechanisms are neglected. The estimated energy distributions of the densities of bulk traps in HTV silicon rubber samples, using equations (4.3) – (4.5) and decay rates measured at ~300 mbar, are shown in Figure 4.17. As can be seen, the characteristic energy of traps is within the range of 0.85-0.98 eV, which is defined by the experimental conditions, and their densities are in order of $10^{18} \text{ eV}^{-1}\text{m}^{-3}$. One should note that the density of trap states obtained from the surface potential decay characteristics is proportional to the density of trapped charges [63]. Since it is probable that not all traps in the material are being occupied, the obtained values may be underestimated. It is notable that the obtained energy distributions of traps correlate well with materials bulk conductivities. Thus, the energy corresponding to the maximum of the trap states is higher for the materials with lower conductivity. The shallowest traps are found in material D (most conductive) with the energy of the maximum of the density below 0.84 eV while the deepest traps are in material B (most resistive) with the maximum density expected at energies higher than 1 eV. This tendency is also valid for other materials, observe Figure 4.15 and Figure 4.17. Hence, the progressive increase in the energy depth of the trap states lead to a reduced bulk conductivity, increased stability of trapped carriers [26] and weaken effect on the non-linear bulk conductivity (Figure 4.15). All these factors result in a slower potential decay (Figure 4.14).

Concerning the polarity effect, it can be noticed that the absolute differences in energy distributions of positive and negative traps for all the material samples are very small. The only visible difference can be seen for material D and correspondingly its effect on the decay characteristics and bulk conductivity.

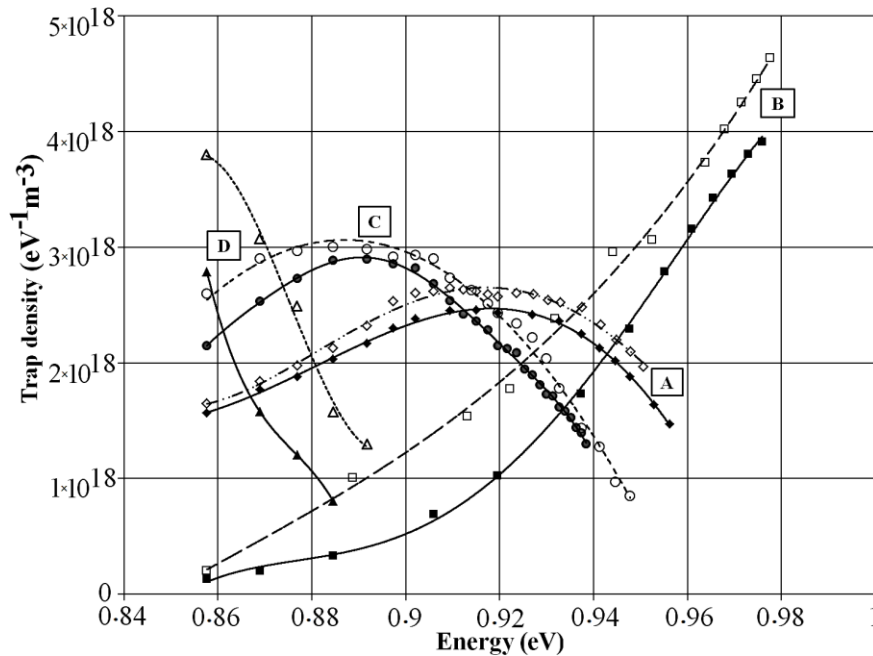


Figure 4.17. Energy distribution of the trap states for different materials deduced from the measured decay characteristics. Solid lines represent the positive traps while dotted lines are the negative traps.

5. Potential decay modeling

This chapter focuses on simulation of potential decay model, accounting for charge leakage through material bulk and along gas-solid interface. The experimentally performed decay measurements on pre-charged HTV silicon rubber surfaces are compared with the output from the performed simulations. Results of a parametric study aiming at identifying the influences of the volume and surface conductivities of the materials as well as the effect of a space charge in the bulk on surface potential decay are examined. Field dependent bulk conductivities obtained from potential decay characteristics for the studied material samples are used as a parameter to get the best fit of the experimental and simulation results.

5.1 Physical background and computer implementation

Charge/potential decay on insulating materials occurs due to the transvers (surface) and longitudinal (bulk) conductivities of the solid material and neutralization caused by the conduction of ions within the gas phase. Under normal conditions, all the three decay mechanisms act simultaneously and it is a difficult task to distinguish between their individual contributions to the total effect. In the present study, the influence of gas phase is eliminated by considering the dynamics of surface potentials at reduced gas pressure that provides a low number of ions in the gas volume, as shown in Figure 4.5. Such approach allows for analyzing solely the role of solid material on the surface charge behavior, which can be affected by several processes in the solid, e.g., dipolar relaxation, induced conductivity, dispersive transport and slow de-trapping [15, 25]. Furthermore, for the studied HTV silicon rubber samples, the experimentally obtained surface charge/potential decay curves were fitted with exponential and power time laws. The resultant characteristics, shown in section 4.4, indicated that for most of the materials, intrinsic conduction is mainly responsible for surface charge dynamics and other mechanisms such as charge injection, slow bulk polarization, etc. are negligible for the conditions of the present study. In order to further analyze the influences of volume conductivities as well as to suggest relevant parameters at which the contribution of space charges and surface conduction may be considerable, potential decay model presented earlier in section 2.4 (equation (2.11)) was utilized.

Equation (2.11) was solved numerically using simulation tool Comsol Multiphysics, which is based on finite element method. The equation was implemented in a 1D axially symmetric model as the measured surface potential distributions were found to be symmetrical around the mid position of the sample (location of the tip of the corona needle). In the selected 1D approach, the computational domain (line) represented the gas-solid interface and all the material parameters were taken as being independent of the sample thickness. The coefficients in (2.11) were calculated using characteristics of the material samples shown in Table 3.2, the mobility value $\mu = 10^{-14} \text{ m}^2\text{V}^{-1}\text{s}^{-1}$ was adopted from [64], and the surface potential profile measured immediately after the gas evacuation (3 min after charging) was used as the initial condition.

5.2 Comparison of the experimental and simulation results

The experimentally obtained potential distributions at different time instants during the decay process and the output from the simulations are shown in Figure 5a and Figure 5b for materials E and B, respectively. Recall that material E is in general more conductive than B (compare the properties in Table 3.2). As it was already mentioned in section 4.4, the lateral spread of the charged spots on surfaces of the materials is negligible even at long times after charging that leads to the conclusion that the contribution from surface conduction to the charge decay is insignificant. Hence, the observed time variations of the surface potential are affected mainly by bulk conduction. This is also confirmed by the results of the simulations shown in Figure 5.1 by broken lines. As can be seen, the calculations yielded similar tendency in the time evolution of the potential profiles as observed in the experiments. However, quantitatively the agreement is poor, especially at the long instants. Thus in Figure 5.1b, the distribution calculated for 337 min is almost overlapping with the experimental profile for 577 min indicating that the actual

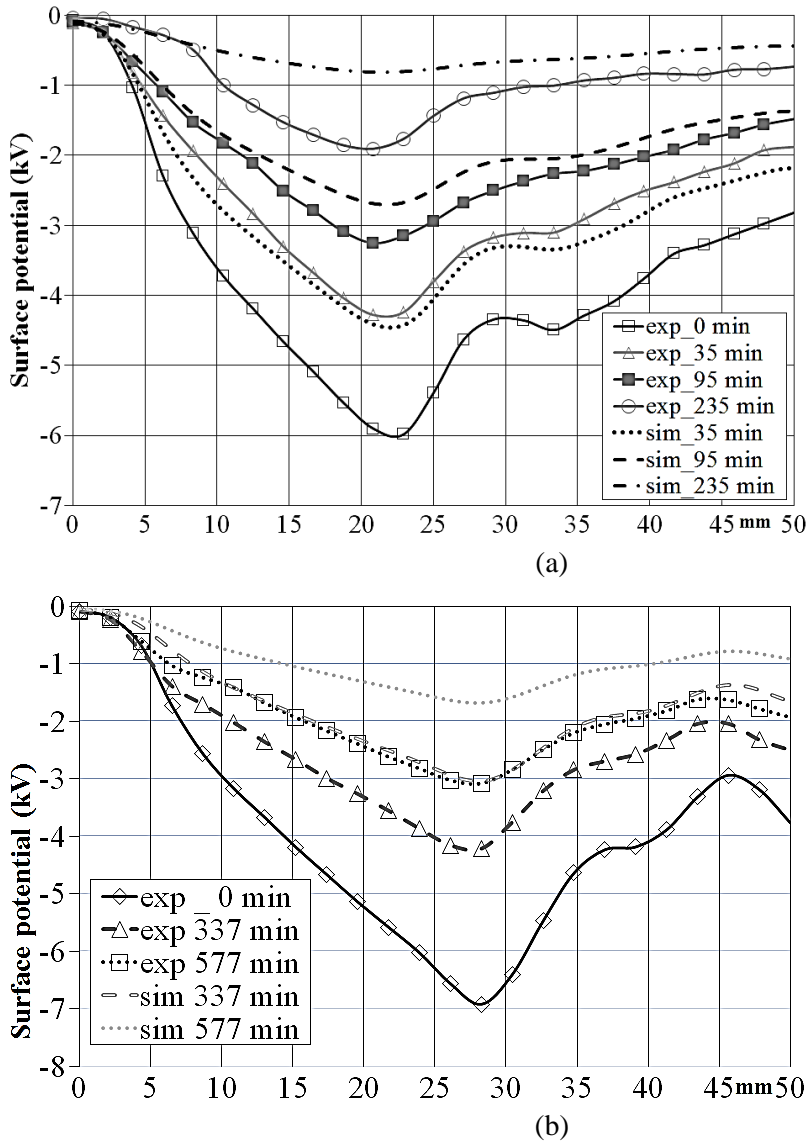


Figure 5.1. Measured and simulated surface potential profiles on E (a) and B (b) materials at 300 mbar at different times after charging.

potential decay is much slower than the calculated one. The discrepancies may arise due to the fact that the fixed conductivity values from Table 3.2 obtained at 1 kV test voltage were used in the simulations. In the experiments, however, the electric field in the material induced by the deposited surface charges may become strong enough to activate field-dependent conduction mechanisms in the bulk. In this case, taking into account that the measured potentials (and thus charges) are unevenly distributed along the surface, one can expect a certain dependence of the bulk conductivity on the location on the sample surface. This allows to suggest that field-dependent conductivities, as shown in Figure 4.15, should be used in (2.11) instead of the constant values. Results of the implementation of this hypothesis in the model are presented below.

5.3 Effects of material properties on surface potential decay

5.3.1 Analysis of effect of bulk conductivity

The influence of the bulk conductivity on surface potential decay can be identified by comparing the dynamic behavior of the potential distributions shown in Figure 5.2. The characteristics are presented for the materials with significant differences in the bulk conductivity and are arranged in such a way that its overall level decreases from plot (a) to (c). As it is observed, the higher the conductivity of the material leads to the faster potential decay. For material D, the conductivity is highest among all the studied ones and the surface potential vanishes within tens of minutes (Figure 5.2a). At the same time, the much lower conductivity of material B (almost two orders of magnitude) yields a very long decay time and it takes ~ 10 hours for the maximum of V_s to reach a half of its initial value (Figure 5.2c). It is notable that the increase in the conductivity only enhances the potential decay rate while the shapes of the profiles are not modified.

The plots in Figure 5.2 also demonstrate the results of the performed simulations, by accounting for the field dependent bulk conductivities and using the potential values measured at 300 mbar immediately after completing gas evacuation as the initial conditions (marked as 0 min in the plots). In this case incorporating the dependencies $K_v(V_s)$ from Figure 4.15 into the model yielded good agreement between the computed and measured distributions. Recall that the profiles did not match when constant conductivities were used (compare Figures 5.1b and 5.2c).

5.3.2 Contribution of surface conduction to potential decay

A parametric computational study was performed in order to analyze the influence of surface conductivity on surface potential profiles as well as on the potential decay. In the calculations, the bulk conductivity 10^{-15} S/m and the thickness of the material sample 2 mm were used that corresponded to B material, the least conductive one. The curve marked as “0 min” from Figure 5.2c represented the initial conditions. The computed variations of surface potential profiles obtained with two different values of surface conductivity are shown in Figure 5.3 for two instants after charging. It was found from the simulations that for the given conditions, the influence of surface conductivity could only be feasible when its magnitude exceed $\sim 10^{-17}$ S. As it is shown in the figure, the enhanced surface conduction intensifies charge spreading along the surface and may even result in a crossover of the surface potential profiles (curves for $K_s = 10^{-15}$ S). It also could yield a faster potential decay (note that the measured surface conductivity for B material is equal to $5 \cdot 10^{-19}$ S, Table 3.2).

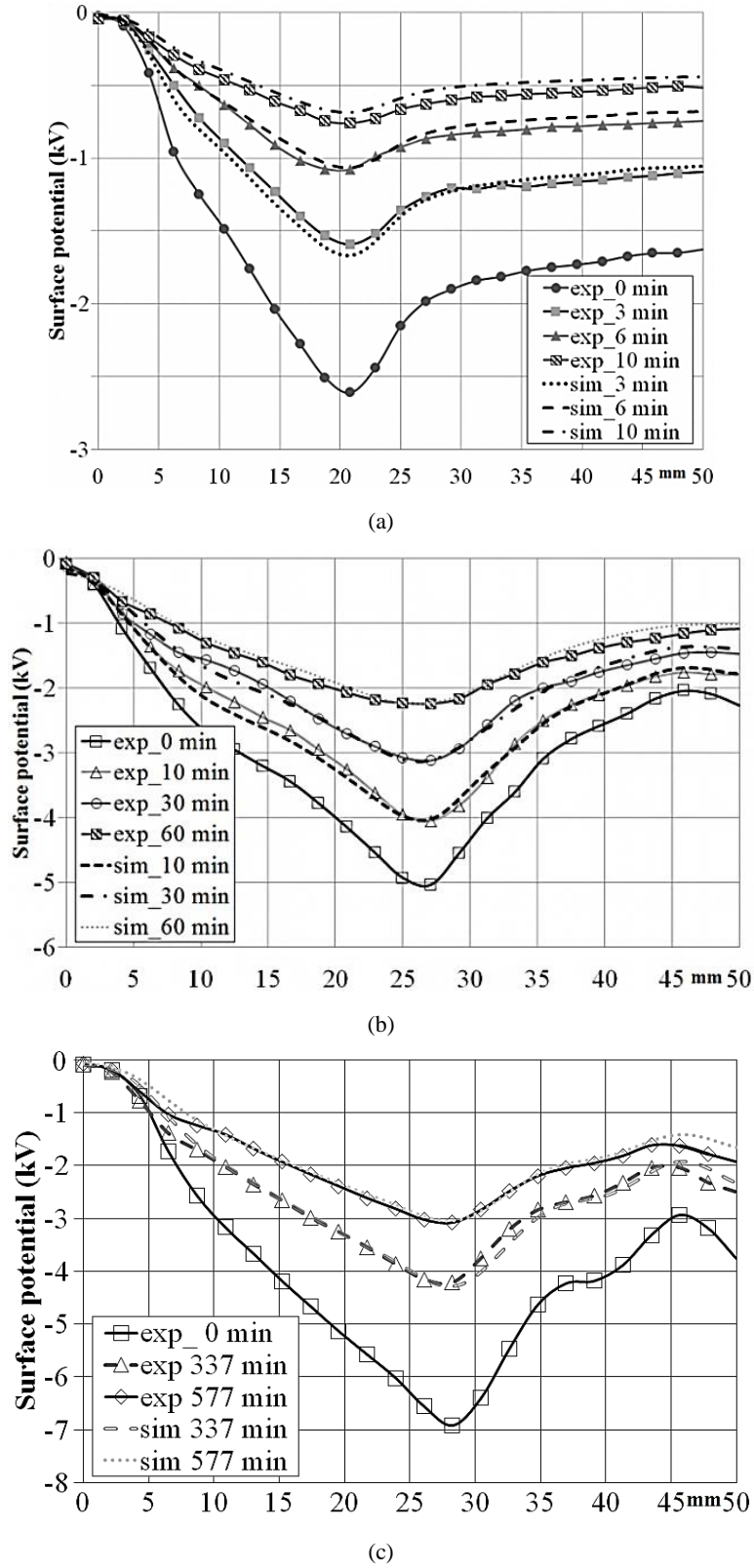


Figure 5.2. Measured and simulated surface potential profiles for D (a), A (b) and B (c) materials at 300 mbar at different times after charging, the results of the simulations were obtained with the model accounting for the field dependent conductivity.

5.3.3 Space charge effect

As follows from (2.11), the space charge limited current may be another factor influencing charge/potential dynamics on material surface. Assuming that its origin in a material is related to presence of trapping states, its magnitude is given by [46, 47].

$$J_{SC} = \frac{9}{8} \mu \epsilon_0 \epsilon_r \theta \frac{V^2}{L^3} \quad (5.1)$$

where factor θ is defined as

$$\theta = \frac{N_c}{N_t} \exp\left(-\frac{(E_c - E_t) - \beta\sqrt{E}}{kT}\right) \quad (5.2)$$

Here, N_c and N_t are the density of states and $(E_c - E_t)$ is the energy gap between the conduction and trap states, $\beta\sqrt{E}$ accounts for Poole-Frenkel effect.

To evaluate the SCLC, information about densities of traps is needed, which is provided in Figure 4.17. By considering equation (5.2), one may notice that the SCLC in the material is strongly field-dependent. The electric field induced by deposited surface charges can lower the electrostatic barrier of the trapped carriers [47] causing de-trapping. This leads to an increase in the SCLC (due to increased θ , see equation (5.1)) and, as a consequence, enhances the surface potential decay according to (2.11). Thus, this mechanism becomes more efficient at higher field strengths which is achieved at higher surface potentials and smaller thickness of material samples [45, 47]. Thus in [45], the SCLC regimes has been reported at ~ 950 V and material thickness of $27 \mu\text{m}$. Taking all these into account, it is hard to expect that SCLC can be significant under conditions of the present study. Estimations showed that the space charge effect may important only for thin films of the materials with thicknesses below $\sim 100 \mu\text{m}$.

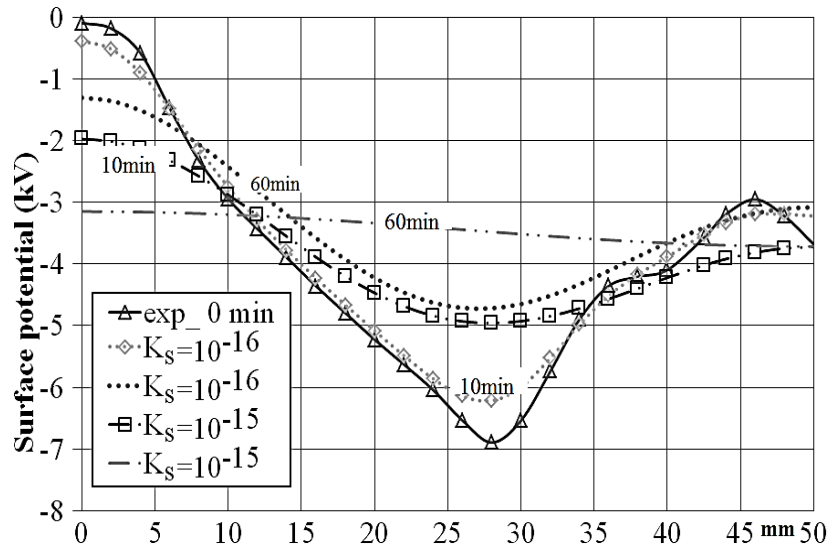


Figure 5.3. Simulated distributions of surface potential at different times after charging and various surface conductivities.

6. Surface charge/potential decay on XLPE

Cross-linked polyethylene (XLPE) is among one of those materials that are used in cable insulation and other high voltage applications due to its excellent electrical properties in particular extremely high resistance. This chapter focuses on electrical characterization and understanding of physical mechanisms responsible for potential decay on flat XLPE samples. The influence of different parameters like air pressure and material properties on the charge decay is evaluated. Field dependent bulk conductivity and energy distribution of trap states deduced from the measured potential decay characteristics are presented and discussed.

6.1 Electrical conductivity and dielectric response of XLPE

Surface and volume currents obtained for XLPE, using Keithley 6517A electrometer equipped with a resistivity test fixture 8009, are shown in Figure 6.1. As can be seen, the variations with respect to measuring time are different for surface and bulk currents. The bulk current, after a time span of 1000 sec, drops down to the noise level which indicate that volume conductivity is extremely low. On the other hand, surface current after the relaxation of initial polarization processes, activated as a result of applied test voltage of 1kV, reach a fairly constant value of approximately $2.54 \cdot 10^{-13}$ A. Fluctuations on the top of the steady state surface current may be either due to the surrounding noise or experimental setup. The obtained conductivities are given in Table 6.1.

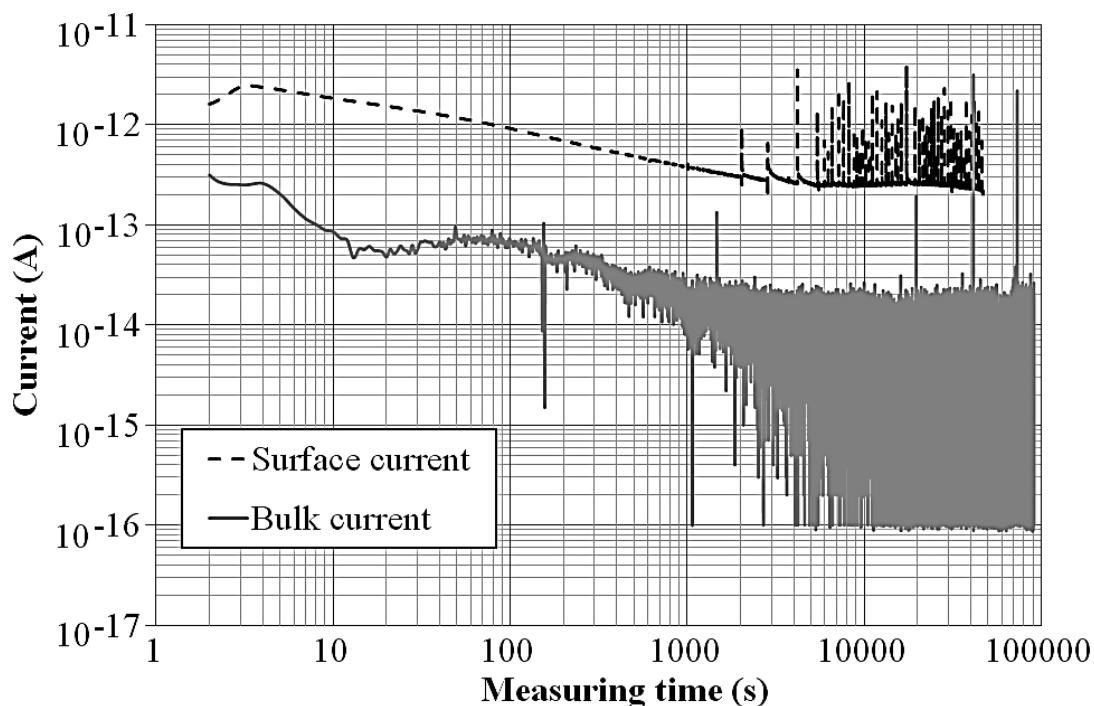


Figure 6.1. Surface and volume current for XLPE.

Table 6.1. Electrical characterization and thickness of XLPE (a and b are to be found from the lowest measured current magnitude).

Material	K_v , S/m	K_s , S	ϵ_r	L, mm
XLPE	$< a \times 10^{-b}$	4.8×10^{-18}	2.2	2.1

Real and imaginary parts of the complex permittivity measured at different frequencies of the applied test voltage using Insulation Diagnostic System IDAX 300 are shown in Figure 6.2. As

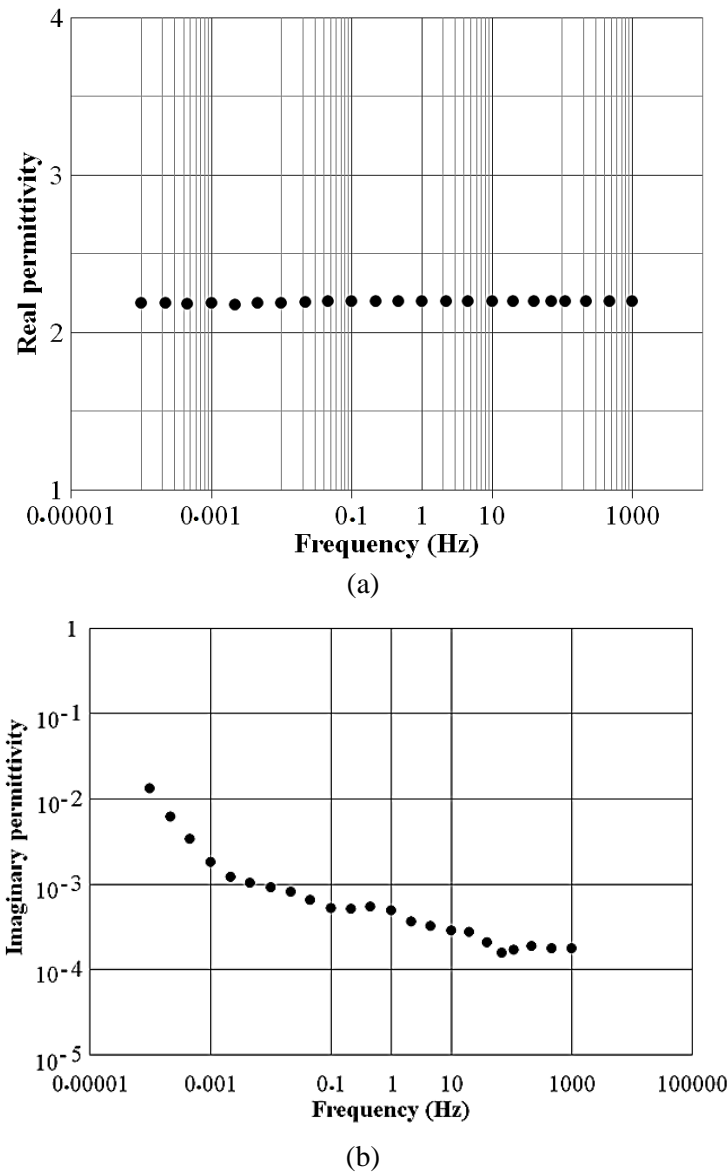


Figure 6.2. Real (a) and imaginary (b) parts of complex permittivity of XLPE.

can be seen, the real part is nearly constant in the overall frequency window indicating that polarization phenomena don't change in the selected frequency range. The imaginary part of complex permittivity, which represents losses in the material, is shown in Figure 6.2b. As seen, higher dielectric losses appear at lower frequencies and they decrease with increasing frequency. The obtained material properties of XLPE are given in Table 6.1.

6.2 Surface potential decay on XLPE at different air pressures

Potential distributions measured at different time instants during the decay process at two air pressures are shown in Figure 6.3. As can be seen, with the passage of decay time not only the maximum magnitude of surface potential decreases, but also, there exist a lateral spread of the charges along the material surface since bulk conductivity of XLPE is extremely low as described in the previous section. Therefore, charges may not escape through the material bulk and physical processes in the bulk may not be considered as a major contribution to the potential decay. Instead, the tangential component of the electric field induced by deposited charges activates surface conduction that causes their lateral spreading. Also at normal pressure, due to the arrival of free counter ions present in the surrounding volume, surface charges are neutralized that, however, requires relatively long times. The effect of these two mechanisms causes a decrease in the magnitude of surface potential, particularly at the location corresponding to the peak value. Further, at 300 mbar air pressure, gas neutralization is insignificant and thus, charge decay may be more or less attributed to surface conduction only. The latter effect that causes the potential on the material surface to approach to a nearly uniform value can be clearly observed for potential profiles recorded for long times after charging.

In addition, according to equation (2.1), potential distributions provide direct images of the surface charge densities. Therefore, there is no way for deposited charges to escape from the surface at reduced air pressure. Hence, the area under each curve that gives the total accumulated charge remains almost the same as seen in Figure 6.3b for longer instants.

Decay of the maximum magnitude of surface potential

Normalized surface potential decay characteristics obtained for the locations corresponding to the maximum values of V_s are shown in Figure 6.4. Comparing the characteristics for different pressures, it can be observed that the decay process takes longer time at reduced air pressure. Thus, the time needed for the reduction of the potential down to 50% of its initial value at ~300 mbar is nearly 100 h longer as compared to that at atmospheric pressure. The reason could be due to the fact that the former provides a significant decrease in the number of free ions in the gas phase, as shown in Figure 4.5, and thus, strongly minimizes the intensity of gas neutralization. Under these conditions, charge decay is solely considered due to material properties. Further, due to extremely low electrical conductivity the decay process is very slow and, consequently, for the maximum potential to reach to half of its initial value, the required time is approximately 300 hours. The polarity of the deposited charges does not seem to affect the decay process significantly (compare corresponding curves in Figure 6.4a and 6.4b).

As seen from Figure 6.4, the potential decays faster at the beginning of the process when its magnitudes are relatively high. This is clearly seen in Figure 6.5 where the decay rates, dV_s/dt deduced from the measured characteristics are presented. As can be seen, the decay rates are affected by the magnitude of the surface potential, material properties and amount of ions present in the gas phase. The higher the surface potential and the amount of ions in air, the higher is the

decay rate and vice versa for lower surface potential and reduced amount of ions. Further, the absolute differences in the decay rates for XLPE at different air pressures are comparatively larger than for HTV silicon rubber samples, described in section 4.4, due to its extremely low electrical conductivity.

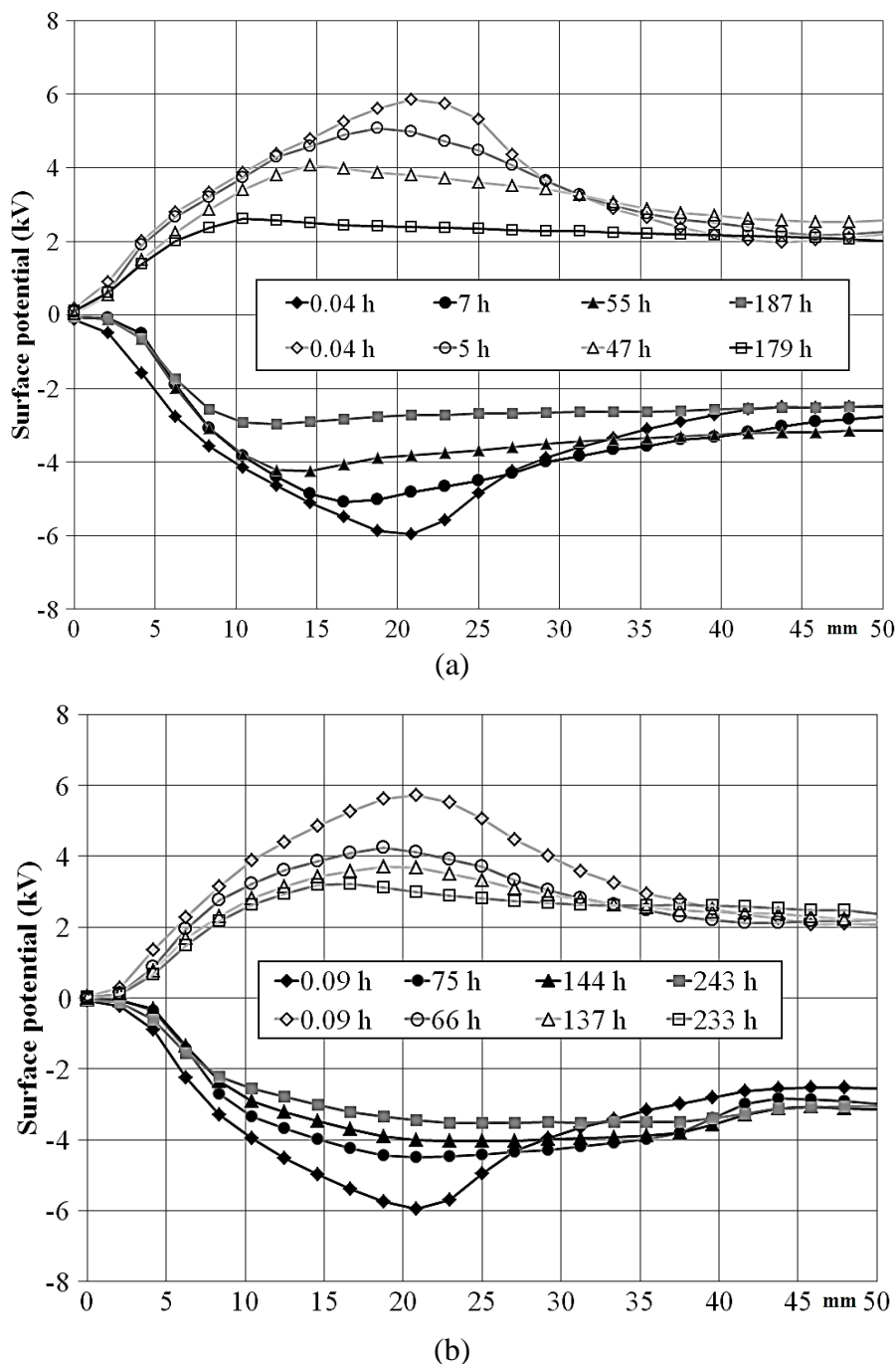
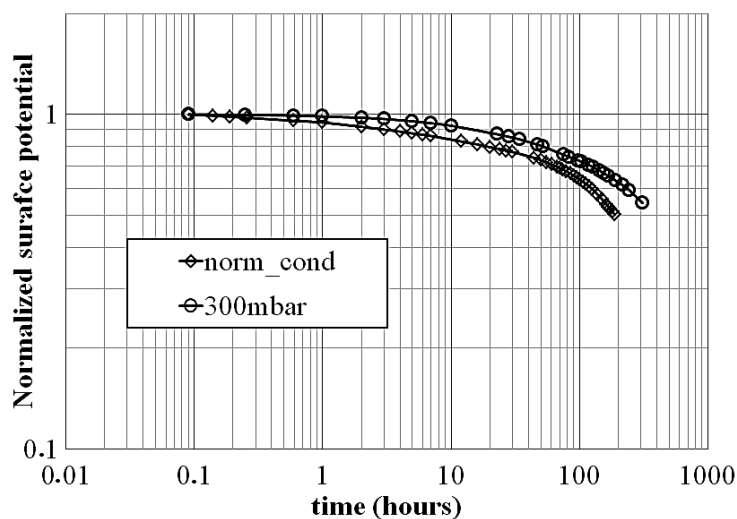
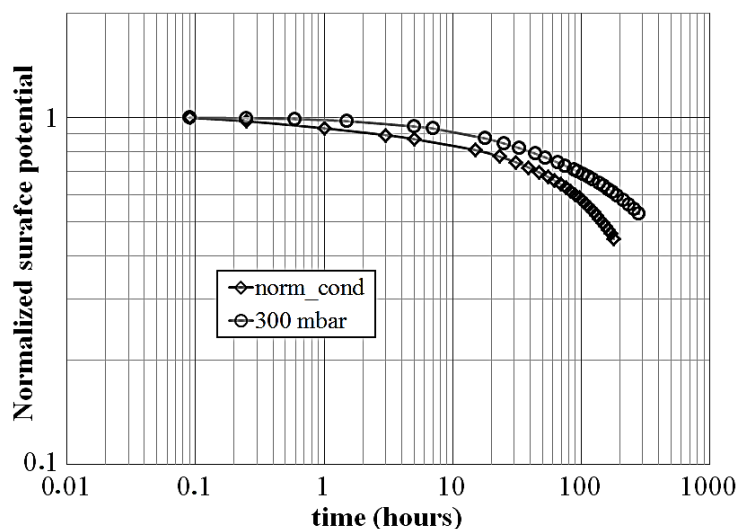


Figure 6.3. Measured surface potential distributions at different time instants during the decay process on XLPE at normal (a) and 300 mbar (b) air pressure.



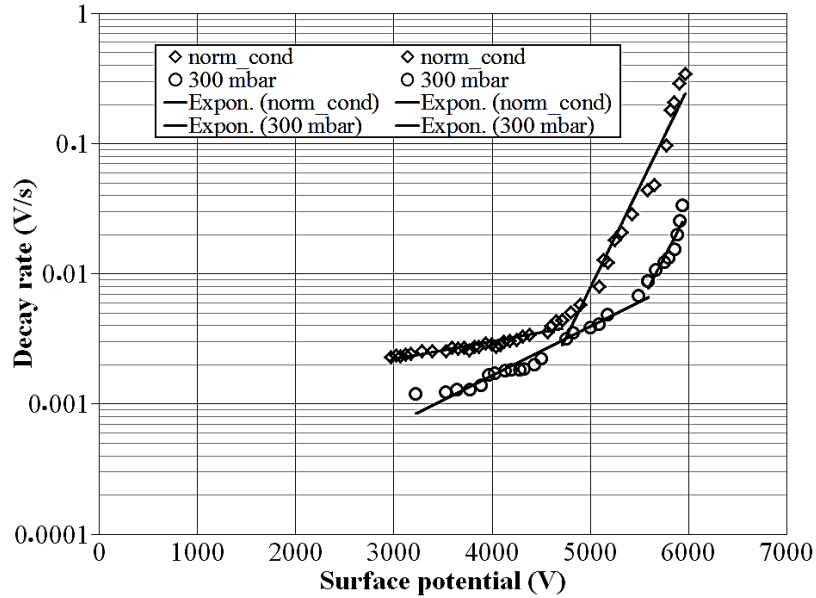
(a)



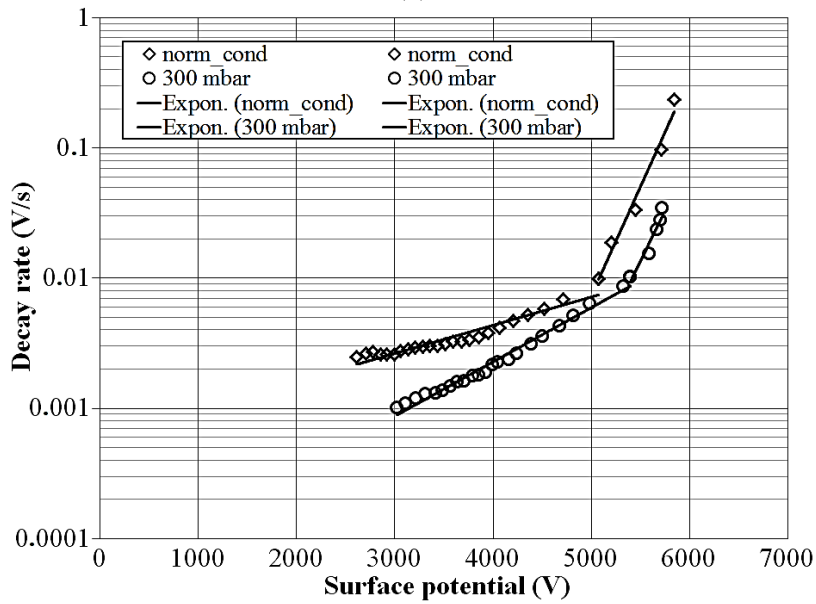
(b)

Figure 6.4. Surface potential decay characteristics for different materials at different air pressures for (a) negative and (b) positive charging. The surface potential is normalized to its maximum value corresponding to the first measured point.

It can be noticed from the figures that the rates of the potential decay for both polarities and both studied pressures follow exponential behavior. Each set of data points, obtained under the similar experimental conditions are best fitted by two exponential functions having different slopes, Figure 6.5. This suggests that the arrival of free counter ions to neutralize the deposited surface charges can only enhance the decay rate, particularly at higher induced electric fields in the surrounding volume, without modifying the profiles of the decay characteristics to a large extent. Based on these observations, one may suggest that gas neutralization, at least for the present study, is not significant as compared to other charge decay mechanisms.



(a)



(b)

Figure 6.5. Decay rates of surface potentials at (a) negative and (b) positive charging for XLPE utilizing maximum V_s values measured at different air pressures. Solid lines are the fitting of the experimental points.

6.3 Field dependent bulk conductivity and trap density distribution in XLPE deduced from surface potential decay characteristics

Charge dynamics measured on surface of XLPE sample can be used to extract materials properties such as field dependent bulk conductivity and energy distributions of the trap states.

Although, it is important to mention here that for obtaining such parameters it is necessary that charge decay should be dominantly affected by bulk processes which is found to be not the case for XLPE. Nevertheless, an attempt has been made to get a rough estimation of the volume conductivity using Poole-Frenkel model. Similarly, an image of energy distributions of the traps states has been obtained which may not be purely allocated to the bulk of material, rather it can be considered to a thin surface layer where partial charge injection may take place.

Field dependent bulk conductivities

Field dependent bulk conductivity of XLPE deduced from the data in Figure 6.5 utilizing the model (2.5) - (2.7) is shown in Figure 6.6. The experimentally obtained data points are fitted by solid lines that vary exponentially with the magnitude of surface potential. Such dependences of the bulk conductivity may occur in general due to activation of the field assisted mechanisms inside the material bulk e.g. charge trapping and de-trapping, space charge accumulation, etc. However for the case of XLPE, exponential variations may not be purely attributed to such physical processes. This is further confirmed by the parameters given in Table 6.2 obtained as a result of exponential fitting utilizing Poole-Frenkel model. As seen, there are large discrepancies between the experimental and theoretical values of β . Since, exponential factor β represent an overall effect of the field assisted mechanisms inside the material bulk, its significant deviation

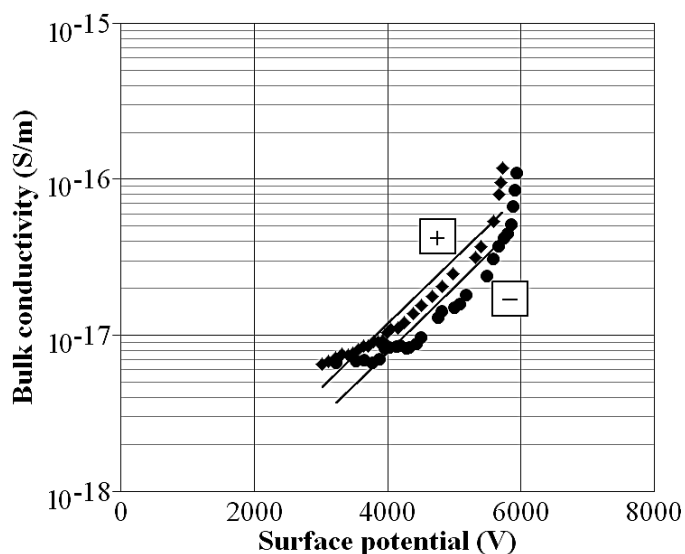


Figure 6.6. Field dependent bulk conductivities deduced from the measured surface potentials. Filled markers fitted by solid lines represent the exponential dependence of the conductivity.

Table 6.2. Parameters of Poole-Frenkel model. The symbols represent the respective polarity.

Parameter		
$K_{v0} \text{ -/+}$	$\beta \text{ experimental} \times 10^{-3} \text{ -/+}$	$\beta \text{ theoretical} \times 10^{-3} \text{ -/+}$
$1.72 \times 10^{-17} / 1.57 \times 10^{-17}$	5.642/7.115	43.499

from the theoretical value indicate that Poole-Frenkel model is not capable to describe the non-linear behavior of the bulk conductivity of XLPE. Further, from the exponential fitting, zero-field limit value K_{v0} is estimated which is extremely low. The latter parameter also confirms the measurement of volume current shown in Figure 6.1 and in Table 6.1. As described before, it was not possible to determine the magnitude of the bulk conductivity with standard measuring technique, however, a rough estimation could be obtained from the surface potential decay characteristics.

Trap density distributions

The energy distributions of the densities of traps in XLPE were estimated in a similar manner as for the HTV silicone rubbers using equations (4.3) – (4.5) and decay rates measured at ~ 300 mbar. The results are shown in Figure 6.7. As seen, the characteristic energy of traps is within the range of 0.85 - 1.07 eV, which is defined by the experimental conditions, and their densities are in the range of 1×10^{17} - 3×10^{18} $\text{eV}^{-1}\text{m}^{-3}$. The absolute differences in the energy distributions of positive and negative traps can be hardly seen in the figure. Further, it can be noticed that the obtained trap energy distributions of XLPE can be correlated to its conductivity. Thus, the energy corresponding to the maximum of the trap states is getting higher (the traps become deeper) as the material conductivity gets lower. The peak of the trap density is not reached at the obtained energies. Comparing the energy distributions shown in Figure 6.7 with the ones obtained for silicon rubber samples, it can be found that the energy window is much wider. This leads to relatively weak non-linearity of the bulk conductivity, increased stability of trapped carriers and slowdown in the decay rates [26].

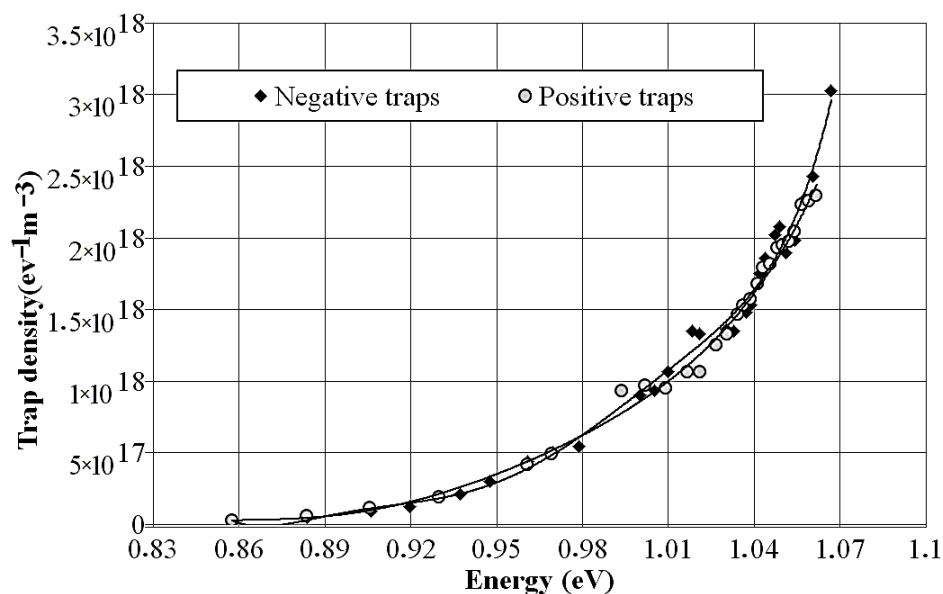


Figure 6.7. Energy distribution of the trap states for XLPE deduced from the measured decay characteristics. Solid lines represent the fitting of experimentally obtained data points.

7. Conclusions

The studies performed within the thesis work were focused on dynamics of surface charges deposited on flat ~2 mm thick HTV silicon rubber and XLPE samples. Effects of different parameters like ambient air pressure and material properties on surface potential distributions and charge decay were investigated. A computer model accounting for charge leakage through material bulk and along gas-solid interface has been developed and output from the simulations was compared with the experimentally obtained potential distributions. Conclusions drawn from each of these studies are summarized below.

Surface charging

Surface potential distribution due to charging by corona in air initiated from a needle located at the center of the sample was found to be bell or saddle-shaped. The latter appeared when charging voltage exceed a certain threshold value. An increase in the voltage amplitude or the needle electrode gap distance result in larger area of charge spot and more spread of surface potential. The material properties can be correlated to the surface charging in such a way that the lower surface and bulk conductivity values result in stronger potential (charge) spread over the surface and its higher is its peak value, respectively. Surface charging at reduced ambient pressure causes a reduction in the maximum magnitude of surface potential which may be allocated to the increase in the intensity of back discharges or to the lower number of free ions in the gas phase. The differences in the peaks of negative and positive surface potentials are within a couple of hundreds of volts that may indicate a weak dependence on the polarity of applied voltage.

Surface charge/potential decay at different pressures of ambient air

Surface potential decay measured at different pressures of ambient air allow for quantifying the role of gas neutralization to the total charge decay as well as to analyze solely the effect of solid material properties on surface charge dynamics. The experiments demonstrated that the amount of ions present in gas affect the charge decay, however, its intensity weakens with the drop in the pressure level inside the test vessel as well as with the decrease of the magnitude of the surface potential. It has been found that gas neutralization causes a visible difference in the decay profiles of material samples with relatively low conductivity. However, the relative contribution to the total charge decay is quite small. The reduction of the ambient pressure to a level of ~300 mbar can significantly decrease the background ions density and thus, surface charge dynamics can be solely considered due to material properties. For the studied material samples, the decay rates are found to have a weak dependence on the polarity of deposited surface charges.

For HTV silicon rubber samples, the measured characteristics of the variations of the potential distributions with respect to decay time are such that there is a decrease in the maximum magnitude of surface potential. However, the shapes of the profiles remain preserved during the decay process which indicated that bulk conduction is the dominant mechanism of the potential decay. Further, with the help of exponential and power time laws, it has been proved that intrinsic

conductivity is the most suitable parameter that fully describes the potential kinetics determined experimentally. On the other hand for XLPE, a lateral spread of the charges along the material surface was observed since the bulk conductivity of XLPE was found to be extremely low. Therefore, current leakage might not take place through the material bulk and consequently, the potential distributions approached a uniform shape at long time after charging.

Evaluation of material properties from potential decay characteristics

Field dependent bulk conductivities for HTV silicon rubber samples deduced from the measured decay rates at reduced air pressure were fitted using Poole-Frenkel model. It has been found that for relatively highly conductive rubbers (D and C), the model provides the best fit and measure of the strength of all physical process that result in the non-linear behavior of the bulk conductivity. They also correlate well with the apparent mobilities of charge carriers and energy distributions of the trap states (the higher mobility and the shallower traps are associated with higher bulk conductivity values). The discrepancies in the experimental and theoretical values of β (Poole-Frenkel factor) were significant for material samples that have low electrical conductivity. For XLPE, it has been found that using Keithley 6517A electrometer it was not possible to measure bulk conductivity even using the highest possible test voltage of 1 kV due to its extremely low value. However, from the measured decay characteristics and utilizing Poole-Frenkel model, a rough estimation can be obtained that may be useful to characterize the material.

Surface potential decay modeling

Potential distributions along the solid material surfaces experimentally obtained during the decay process can provide information related to the transverse or longitudinal transport of charges on the material. The simulation results allowed for evaluating threshold values of the volume and surface electric conductivities at which these transport mechanisms become most essential. Both the experiments and simulations demonstrated that bulk conduction becomes the dominant mechanism of surface potential decay if volume conductivity of the material is above $\sim 10^{-16}$ S/m. The results of the modeling agreed well with the measured characteristics if materials field-dependent conductivities are taken into account. The performed parametric study has also demonstrated that surface conduction may influence the potential decay if its level exceeds $\sim 10^{-17}$ S. The effect of bulk space charges was found to be negligible for the conditions of the present study and its impact on the decay process might be expected at material sample thickness finer than ~ 100 μm .

8. Future work

Possible suggestions for future studies can be an investigation of the effect of ambient temperature variations on surface charge dynamics. Such experiments would provide additional information about surface charge behavior since temperature may influence bulk and surface conduction processes. Further, effect of polarization in the materials can be included. For this, surface potential measurements on material samples charged in a plane electrodes arrangement by applying different voltage shapes may be considered. The analysis of these two factors may further provide a better understanding of physical processes which take place in HVDC insulation and mechanisms responsible for charge dynamics.

The project work related to surface charging and potential decay was performed on flat ~2 mm thick samples of polymeric materials. Similar studies can be performed on thin (in the range of μm) material samples to investigate the possible effects of bulk space charges which were found to be negligible for the dimensions of the presently studied insulation materials.

REFERENCES

- [1] D. Yujian, L. Weiming, S. Zhiyi, L. Qingfeng, G. Chen, and S. Zhaoying, “Switching impulse voltage flashover characteristics of air gaps in ± 800 kV UHVDC transmission tower and altitude correction”, CIGRE, 2012.
- [2] Z. Fang, R. A. Fouracre and O. Farish, “Investigations of surface charging of DC insulator spacers”, IEEE Conf. Elec. Insul. Diel. Phenomena (CEIDP), San Francisco, USA, pp. 149-152, 1996.
- [3] D. K. Das-Gupta, “Surface charge decay on Insulating Films”, IEEE Int. Symp. Elec. Insul., Boston, MA, USA, pp. 296-299, 1988.
- [4] S. Okabe, “Phenomena and mechanism of electric charges on spacers in gas insulated switchgears”, IEEE Trans. Dielectr. Electr. Insul., Vol. 14, No. 1, pp. 46-52, 2007.
- [5] S. Kumara, S. Alam, I. R. Houqe, Y. V. Serdyuk and S. M. Gubanski, “DC flashover characteristics of a cylindrical insulator model in presence of surface charges”, IEEE Trans. Diel. Elec. Insul., Vol. 19, No. 3, pp. 1084-1090, June 2012.
- [6] S. Kumara, “Electrical charges on polymeric insulator surfaces and their impact on withstand performance”, PhD thesis, Chalmers University of Technology, Gothenburg, Sweden, 2012.
- [7] F. Wang, Q. Zhang, Y. Qiu and E. Kuffel, “Insulator surface charge accumulation under DC voltage”, Proc. IEEE Int. Symp. Elec. Insul., pp. 426 – 429, 2002.
- [8] B. Lutz and J. Kindersberger, “Surface charge accumulation on cylindrical polymeric model insulators in air: Simulation and measurement”, IEEE Trans. Diel. Elec. Insul., Vol. 18, No. 6, pp. 240-248, 2011.
- [9] J. A. Giacometti, and O. N. Jr. Oliveira, “Corona charging of polymers”, IEEE Trans. on Electr. Insul., Vol. 27, No. 5, pp. 924-943, 1992.
- [10] K. Nakanishi, A. Yoshioka and Y. shibuya, “Surface charging on epoxy spacer at DC stress in compressed SF6 gas”, IEEE Trans. Power Apparatus Syst. Vol. 102, pp. 3919-3927, 1983.
- [11] C.W. Mangelsdorf and C. M. Cooke, “Static charge accumulated by epoxy post insulation stressed at high DC voltages”, IEEE Conf. Elec. Insul. Diel. Phenomena (CEIDP), pp. 220-227, 1978.
- [12] A. Kumar, D. Wu, R. Hartings and B. Engström, “Experience from first 800 kV UHVDC long-term test installation”, Proc. 6th Int. Conf. Power Trans. Distr. Tech., Guangzhou, China, Nov. 10-12, 2007.
- [13] F. Messerer, M. Finkel and W. Boeck, “Surface charge accumulation on HVDC – GIS – Spacer”, IEEE International Symp. on electr. Insul. , Boston, MA USA, April 7-10, 2002.

- [14] T. Nitta and K. Nakanishi, "Charge accumulation on insulating spacers for HVDC GIS", *IEEE Trans. on Electr. Insul.*, Vol. 26, No. 3, pp. 418-427, 2002.
- [15] P. Molinie, "Measuring and modeling transient insulator response to charging: the contribution of surface potential studies", *IEEE Trans. Diel. Elec. Insul.*, Vol. 12, No. 5, pp. 939-950, 2005.
- [16] P. Molinie, M. Goldman, and J. Gatellet, "Surface potential decay on corona-charged epoxy samples due to polarization processes", *J. Appl. Phys.*, Vol. 28, pp. 1601-1610, 1995.
- [17] E. Kuffel, W.S. Zaengl, and J. Kuffel, "High Voltage Engineering Fundamentals", Pergamon Press, 1984.
- [18] M. M. Shahin, "Nature of charge carriers in negative Coronas", *Appl. Opt. Suppl. Electr. Photogr.*, Vol. 82, pp. 106-110, 1969.
- [19] M. M. Shahin, "Mass – Spectrometric studies of corona discharges in air of atmospheric pressures", *J. Chem. Phys.*, Vol. 43, pp. 2600-2605, 1966.
- [20] R. Toomer, and T.J. Lewis, "Charge trapping in corona-charged polyethylene films", *J. phys. D: Appl. Phys.*, Vol. 13, No. 7, pp. 1343-1355, 1980.
- [21] E.A. Baum, T.J. Lewis and R. Toomer, "Decay of electrical charge on polyethylene films", *J. phys. D: Appl. Phys.*, Vol. 10, No. 4, pp. 487-497, 1977.
- [22] J. Kindersberger and C. Liderle, "Surface charge decay on insulators in air and sulfurhexafluorid – part II: Measurements", *IEEE Trans. Diel. Elec. Insul.*, Vol. 15, No. 4, pp. 949-957, 2008.
- [23] Y. Späck, S. Kumara and S. M. Gubanski, "Charge decay measurements on a polymeric insulation material under controlled humidity conditions", *Nordic Insul. Symp.*, Trondheim, Norway, pp. 149-152, 2013.
- [24] G. Chen, "Anomalous phenomena in solid dielectrics under high electric fields", *IEEE 9th International Conference on the properties and Applications of Dielectric Materials*, pp. 954-960, 2009.
- [25] P. Molinie and P. Llovera, "Surface potential measurement: implementation and interpretation", *IEEE Conf. Publ. No. 473*, 8th Int. Conf. Diel. Materials, Meas. and Appl., pp. 253-258, 2000.
- [26] P. Llovera and P. Molinie, "New methodology for surface potential decay measurements: application to study charge injection dynamics on polyethylene films", *IEEE Trans. Diel. Elec. Insul.*, Vol. 11, No. 6, pp. 1049-1056, 2004
- [27] G. Chen, J. Zhao and Y. Zhuang, "Numerical modeling of surface potential decay of corona charged polymeric material", *IEEE International Conference on Solid Dielectrics (ICSD)*, pp. 1-4, 2010.
- [28] P. Molinie, "A review of mechanisms and models accounting for surface potential decay" *IEEE Trans. Plasma Sci.*, Vol. 40, No. 2, pp. 167-176, Dec. 2012.
- [29] E. A. Baum, T. J. Lewis and R. Toomer, "The lateral spreading of charge on thin films of polyethylene terephthalate", *J. Phys. D: Appl. Phys.*, Vol. 11, pp. 963-977, 1978.

- [30] A. Crisci, B. Gosse, J.P. Gosse and V. Ollier-Duréault, "Surface potential decay due to surface conduction", *J. Appl. Phys.*, Vol. 4, pp. 107-116, 1998.
- [31] J. Kindersberger and C. Liderle, "Surface charge decay on insulators in air and sulfurhexafluorid – part I: simulation", *IEEE Trans. Diel. Elec. Insul.*, Vol. 15, No. 4, pp. 941-948, 2008.
- [32] T. J. M. Gaertner, Th. Stoop, J. Tom, H. F. A. Verhaart and A. J. L. Verhage, "Decay of surface charges on insulators in SF₆", *Proc. IEEE Int. Symp. Elec. Insul.*, Montreal, Canada, pp. 208-213, 1984
- [33] I. W. McAllister, "Decay of charge deposited on the wall of a gaseous void", *IEEE Trans. on Electr. Insul.*, Vol. 27, No. 6, pp. 1202-1207, 1992.
- [34] S. Kumara, B. Ma, Y. V. Serdyuk and S. M. Gubanski, "Surface charge decay on HTV silicone rubber: effect of material treatment by corona discharges", *IEEE Trans. Diel. Elec. Insul.*, 2012, Vol. 19, NO. 6, pp. 2189-2195.
- [35] Y. Liu, Z. An, Q. Yin, F. Zheng, Y. Zhang, "Rapid potential decay on surface fluorinated epoxy resin samples", *J. Appl. Phys.*, Vol. 113, pp. 164105-164105-8, 2013.
- [36] G. Teyessedre and C. Laurent, "Charge transport modeling in insulating polymers: from molecular to macroscopic", *IEEE Trans. Diel. Elec. Insul.*, Vol. 12, No. 5, pp. 857-875, 2005.
- [37] D.L. Chinoglia, G.F. Leal Ferreria, J.A. Giacometti and O.N. Jr. Oliveria, "Corona-triode characteristics: on effects possibly caused by the electronic component", *7th International Symposium on Electrets*, pp. 255-260, 1991.
- [38] T. Blythe and D. Bloor, "Electrical properties of polymers", Cambridge University Press, 2005.
- [39] Dr. Maciej and A. Noras, "Non-contact surface charge/voltage measurements fieldmeter and voltmeter methods", *Trek Application Note*, 2002.
- [40] H. Sjöstedt, "Electric charges on insulator surfaces and their influence on insulator performance", *Licentiate Thesis, Chalmers University of Technology, Göteborg, Sweden*, ISSN 1652-8891, No. 34/2008, 2008.
- [41] P. Llovera, P. Molinie, A. Soria, and A. Quijano, "Measurements of electrostatic potentials and electric fields in some industrial applications: Basic principles", *Journal of Electrostatics*, Vol. 67, pp. 457–461, 2009.
- [42] D. Min, M. Cho, A. R. Khan and S. Li, "Surface and volume charge transport properties of polyimide revealed by surface potential decay with genetic algorithm", *IEEE Trans. Diel. Elec. Insul.*, Vol. 19, No. 2, pp. 600-608, 2012.
- [43] V. Adamec and J. H. Calderwood, "The interpretation of potential decay on the surface of a charged dielectric specimen", *J. Phys. D: Appl. Phys.*, Vol. 20, pp. 803-804, 1987.
- [44] M. Ieda, G. Sawa and S. Kato, "A consideration of Poole-Frenkel effect on electric conduction in insulators", *J. Appl. Phys.*, Vol. 42, pp. 3737-3740, 1971.

- [45] D. Min, M. Cho, A. R. Khan and S. Li, "Charge transport properties of dielectrics revealed by isothermal surface potential decay", *IEEE Trans. Diel. Elec. Insul.*, Vol. 19, No. 4, pp. 1465-1473, 2012.
- [46] M. A. Lampert, "Simplified theory of space charge limited currents in an insulator with traps", *Phys. Rev.* Vol. 103, No.6, pp. 1848-1656, 1956.
- [47] T. Breuer, U. Kerst, C. Biot, E. Langer, and H. Ruelke et al., "Conduction and material transport phenomena of degradation in electrically stressed ultra low-k dielectric before breakdown", *J. Appl. Phys.* , Vol. 112, 124103, 2012.
- [48] T. A. Burr, A. A. Seraphin, E. Werwa and K. D. Kolenbrander, "Carrier transport in thin films of silicon nanoparticles", *Phys. Rev. B*, Vol. 56, pp. 4818-4824, 1997.
- [49] W. S. Zaengl, "Dielectric spectroscopy in time and frequency domain for HV power equipment, part 1: Theoretical Considerations", *IEEE Electr. Insul. Magazine*, Vol.19, No. 5, pp. 5-19, 2003.
- [50] V. D. Houhanessian and W. S. Zaengl, "Time domain measurements of dielectric response in oil-paper insulation systems", *IEEE Symp. Electr. Insul.*, Vol. 1, pp. 47-52, 1996.
- [51] B. Oyegoke, P. Hyvonen, M. Aro and N. Gao, "Applications of dielectric response measurement on power cable systems", *IEEE Trans. Diel. Elec. Insul.*, Vol. 10, No. 5, pp. 862-873, 2003.
- [52] U. Hõrrak, "Air ion mobility spectrum at a rural area", PhD thesis, University of Tartu, Tartu, Estonia, 2001.
- [53] S. Pancheshnyi, "Role of electronegative gas admixtures in streamer start, propagation and branching phenomena", *Plasma Sources Sci. Technol.*, Vol. 14, pp. 645–653, 2005.
- [54] M.A. Abdul-Hussain and K.J. Cormick, "Charge storage on insulation surfaces in air under unidirectional impulse conditions", *IEE Proceedings on Physical Science, Measurement and Instrumentation, Management and Education*, Vol. 134, No. 9, pp. 731-740, 1987.
- [55] C. M. Cooke, "Charging of insulator surfaces by ionization and transport in gases", *IEEE Trans. Elec. Insul.*, Vol. EI 17, No. 2, pp. 172-178, 1982.
- [56] D. K. Das-Gupta, "Conduction mechanisms and high-field effects in synthetic polymers", *IEEE Trans. Diel. Electr. Insul.*, Vol. 4, No. 2, pp. 149-156, 1997.
- [57] M. M. Perlman, T. J. Sonnonstine and J. A. St. Pierre, "Drift mobility determinations using surface-potential decay in insulators", *J. Appl. Phys.*, Vol. 47, pp. 5016 – 5021, 1976
- [58] Anh. T. Hoang, "Electrical characterization of partial discharge resistant enamel insulation", Licentiate thesis, Chalmers University of Technology, Gothenburg, Sweden, 2014.
- [59] W. W. Shen, H. B. Mu, G. J. Zhang, J. B. Deng, and D. M. Tu, "Identification of electron and hole trap based on isothermal surface potential decay model", *J. Appl. Phys.* , Vol. 113, 083760, 2013.

- [60] W. Shen, G. Wang, Y. Niu, J. Wang, L. Zhang, Y. Zhang and G. Zhang “The energy distribution of traps in polymers based on isothermal surface potential decay measurement”, Int. Conf. High Voltage Eng. and Appl., Shanghai, China, September 17-20, 2012.
- [61] J. G. Simmons and M. C. Tam, “Theory of isothermal currents and the direct determination of trap parameters in semiconductors and insulators containing arbitrary trap distributions”, Phys. Rev. B, Vol. 7, pp. 3706-3713, 1973.
- [62] J. G. Simmons and J. W. Taylor, “High-field isothermal currents and thermally stimulated currents in insulators having discrete trapping levels”, Phys. Rev. B, Vol. 5, pp. 1619–1629, 1972.
- [63] T. C. Zhou, G. Chen, R. J. Liao and Z. Xu, “Charge trapping and detrapping in polymeric materials: trapping parameters”, J. Appl. Phys., Vol. 110, 043724, 2011.
- [64] S. Le Roy, G. Teysseire and C. Laurent, “Charge transport and dissipative processes in insulating polymers: experiments and model”, IEEE Trans. Dielect. Elec. Insul., Vol. 12, No. 4, pp. 644-654, 2005.